Article

Cell Stem Cell

Apelin$^+$ Endothelial Niche Cells Control Hematopoiesis and Mediate Vascular Regeneration after Myeloablative Injury

Graphical Abstract

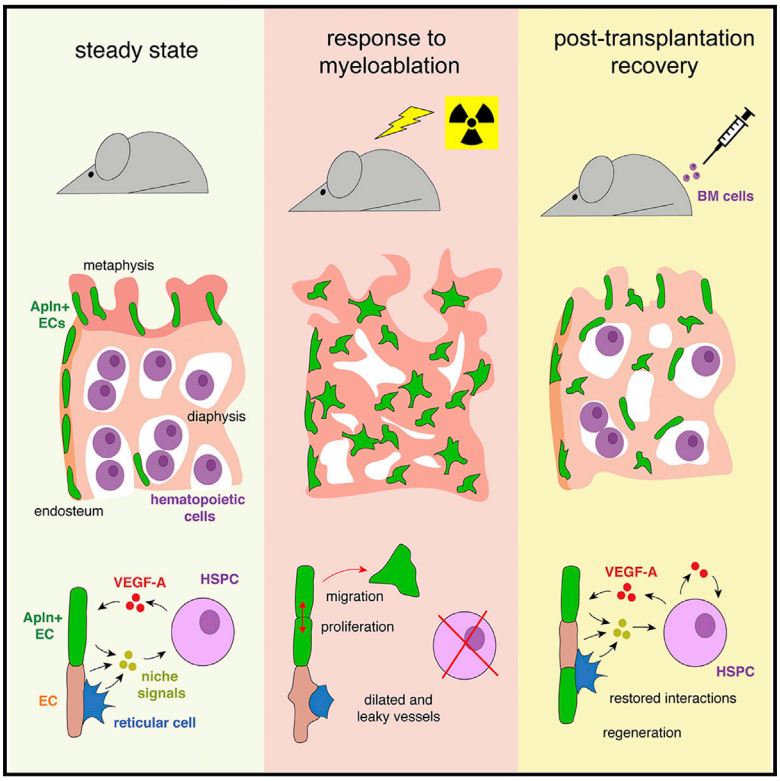

Highlights

- Loss of hematopoietic cells phenocopies irradiation-induced vascular defects
- Identification and characterization of Apln$^+$ ECs in adult BM
- Apln$^+$ ECs regulate HSC maintenance and steady-state hematopoiesis
- Apln$^+$ ECs expand, respond to HSPCs, and drive post-transplantation recovery

Authors

Qi Chen, Yang Liu, Hyun-Woo Jeong, Martin Stehling, Van Vuong Dinh, Bin Zhou, Ralf H. Adams

Correspondence

ralf.adams@mpi-muenster.mpg.de

In Brief

Chen and colleagues identify an Apln$^+$ subpopulation of bone marrow endothelial cells (ECs), which are distinct from other sinusoidal ECs. Apln$^+$ ECs regulate HSC maintenance, hematopoiesis, hematopoietic reconstitution, and vascular regeneration after irradiation. Crosstalk between Apln$^+$ ECs and donor-cell-derived VEGF-A can be manipulated to improve bone marrow transplantation efficiency.

Chen et al., 2019, Cell Stem Cell *25*, 768–783
December 5, 2019
https://doi.org/10.1016/j.stem.2019.10.006

CellPress

CellPress

Cell Stem Cell
Article

Apelin$^+$ Endothelial Niche Cells Control Hematopoiesis and Mediate Vascular Regeneration after Myeloablative Injury

Qi Chen,[1,4] Yang Liu,[1,4] Hyun-Woo Jeong,[1] Martin Stehling,[2] Van Vuong Dinh,[1] Bin Zhou,[3] and Ralf H. Adams[1,5,*]

[1]Max Planck Institute for Molecular Biomedicine, Department of Tissue Morphogenesis, and University of Münster, Faculty of Medicine, Röntgenstrasse 20, 48149 Münster, Germany

[2]Electron Microscopy and Flow Cytometry Units, Max Planck Institute for Molecular Biomedicine, Röntgenstrasse 20, 48149 Münster, Germany

[3]State Key Laboratory of Cell Biology, CAS Center for Excellence in Molecular Cell Science, Shanghai Institute of Biochemistry and Cell Biology, Chinese Academy of Sciences, 320 Yueyang Road, A-2112, Shanghai 200031, China

[4]These authors contributed equally

[5]Lead Contact

*Correspondence: ralf.adams@mpi-muenster.mpg.de

https://doi.org/10.1016/j.stem.2019.10.006

SUMMARY

Radiotherapy and chemotherapy disrupt bone vasculature, but the underlying causes and mechanisms enabling vessel regeneration after bone marrow (BM) transplantation remain poorly understood. Here, we show that loss of hematopoietic cells per se, in response to irradiation and other treatments, triggers vessel dilation, permeability, and endothelial cell (EC) proliferation. We further identify a small subpopulation of Apelin-expressing (Apln$^+$) ECs, representing 0.003% of BM cells, that is critical for physiological homeostasis and transplant-induced BM regeneration. Genetic ablation of Apln$^+$ ECs or *Apln-CreER*-mediated deletion of *Kitl* and *Vegfr2* disrupt hematopoietic stem cell (HSC) maintenance and contributions to regeneration. Consistently, the fraction of Apln$^+$ ECs increases substantially after irradiation and promotes normalization of the bone vasculature in response to VEGF-A, which is provided by transplanted hematopoietic stem and progenitor cells (HSPCs). Together, these findings reveal critical functional roles for HSPCs in maintaining vascular integrity and for Apln$^+$ ECs in hematopoiesis, suggesting potential targets for improving BM transplantation.

INTRODUCTION

Irradiation or chemotherapy followed by allogenic stem cell transplantation is a major therapeutic approach for the treatment of leukemia and other malignant and non-malignant diseases (Copelan, 2006; Ferrara et al., 2009; Kondo et al., 2003; Morgan et al., 2017; Rafii and Lyden, 2003; Thomas et al., 1975). High transplantation efficiency is beneficial for both patients and donors (Ballen et al., 2013; Copelan, 2006; Ratajczak and Suszynska, 2016). Hematopoietic stem cell (HSC) engraftment, proliferation, and differentiation are critically regulated by niche microenvironments, which involve endothelial cells (ECs) and vessel-associated mesenchymal cells (Comazzetto et al., 2019; Crane et al., 2017; Ding et al., 2012; Doan et al., 2013a; Greenbaum et al., 2013; Himburg et al., 2018; Hoggatt et al., 2016; Mendelson and Frenette, 2014; Rafii et al., 2016; Ramasamy et al., 2016; Severe et al., 2019; Sugiyama et al., 2006; Zhao et al., 2014). Whereas it is proposed that lethal irradiation triggers acute loss of ECs, vessel dilation or swelling and changes in permeability have been also reported (Bowers et al., 2018; Doan et al., 2013b; Hassanshahi et al., 2017; Himburg et al., 2016; Hooper et al., 2009; Li et al., 2008; Slayton et al., 2007; Zhou et al., 2015). Thus, our understanding of irradiation and chemotherapy-induced vascular damage and the factors promoting regeneration remain insufficient.

In development but also in the adult skeletal system, ECs are heterogeneous and form different subpopulations (Baryawno et al., 2019; Itkin et al., 2016; Kusumbe et al., 2014; Langen et al., 2017; Rafii et al., 2016; Tikhonova et al., 2019). It is unclear whether all capillary ECs are equally important for hematopoiesis and HSC maintenance. Apelin, encoded by gene *Apln*, is a secreted peptide whose function is reported to be redundant with Elabela/Apela (Helker et al., 2015; Ho et al., 2017; Kim, 2014; Kuba et al., 2019). Apelin is primarily secreted from a subset of capillary ECs, namely, Apln$^+$ ECs, which can be genetically targeted by *Apln-CreER* knockin mice (Chen et al., 2016; Liu et al., 2015; Tian et al., 2013). In the growing retinal vasculature, *Apln* expression is enriched in tip ECs at the distal end of vessel sprouts (del Toro et al., 2010). Apln expression also marks highly proliferative ECs in many developing organs (Langen et al., 2017; Liu et al., 2015; Pitulescu et al., 2017), whereas Apln$^+$ ECs largely disappear in the adult vasculature consistent with its quiescent, non-proliferative status (Liu et al., 2015).

Here, we have combined inducible mouse genetics, flow cytometry, RNA sequencing (RNA-seq), and advanced imaging approaches to show that adult Apln$^+$ ECs are critical for the maintenance of steady-state hematopoiesis as well as vascular regeneration and hematopoietic reconstitution after bone marrow (BM) transplantation.

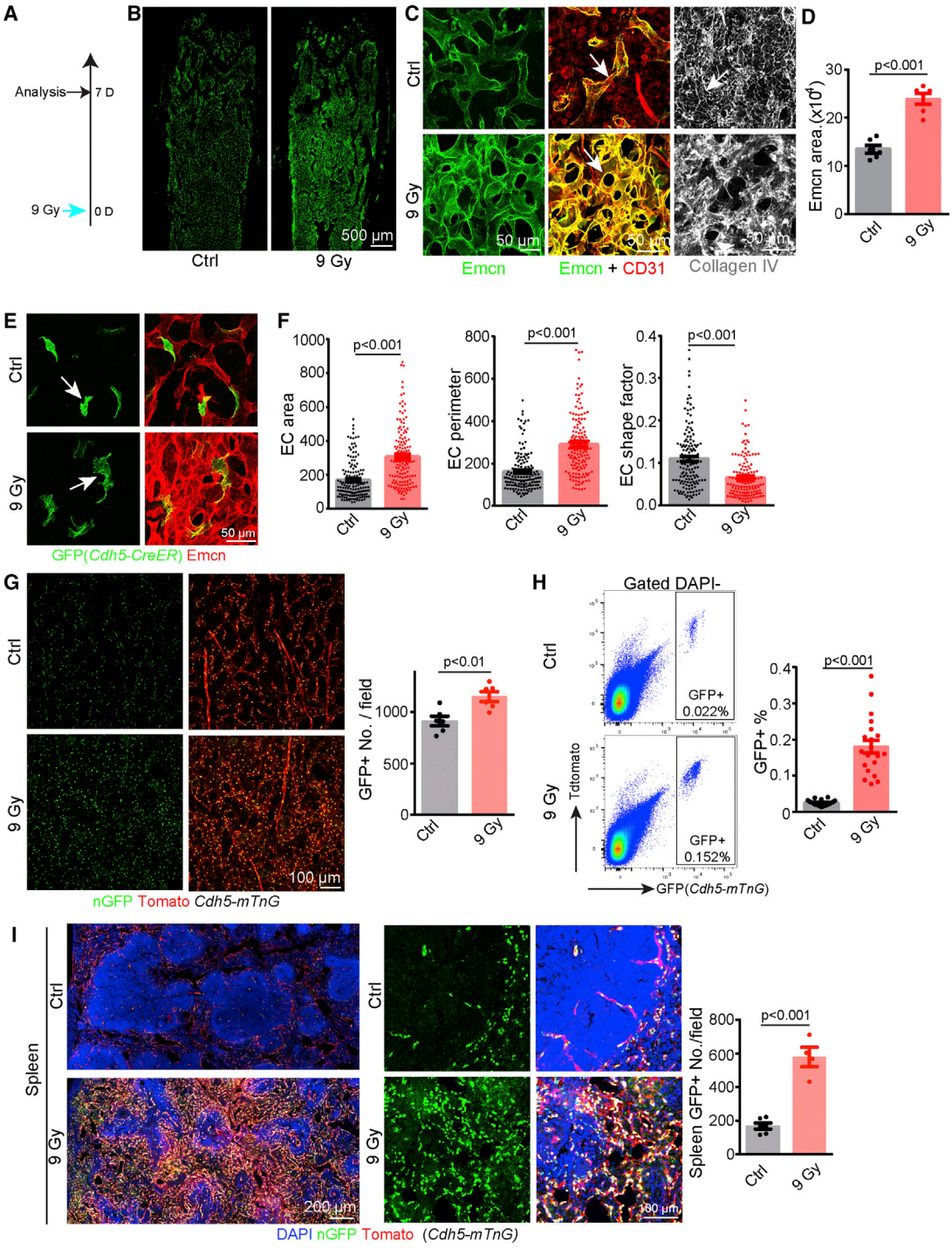

Figure 1. Irradiation-Induced Changes in the Vasculature of BM and Spleen

(A) Schematic representation of protocol for lethal irradiation analysis.

(B) Tile scan overview images of Emcn-stained vessels in adult femur after irradiation.

(C) Emcn, CD31, and collagen IV immunostaining of control and irradiated BM, as indicated. Arrows mark Emcn$^+$ CD31$^+$ vessels in middle panel and collagen IV$^+$ reticular fiber on the right.

(D) Quantification of Emcn$^+$ area in imaging field (n = 6 per group).

(E) Morphology of individual ECs (arrows) in control and irradiated bones of *Cdh5-CreER R26-mTmG* mice. Low dosage of tamoxifen was injected 6 days after irradiation.

(F) Quantification of area, perimeter, and shape factor from control (n = 147 from 3 mice) and 9 Gy (n = 140 from 4 mice) single ECs. Shape factor is a numerical indication of how similar a 2D shape is to a perfect circle, which has a shape factor of 1.

(legend continued on next page)

RESULTS

Irradiation-Induced Changes in Bone ECs

Making use of advanced bone processing and imaging protocols, we found that lethal total body irradiation (9 Gy) of adult mice results in profound alterations of the long bone vasculature at 7 days post-irradiation, including the disruption of columnar capillaries in the metaphysis, dilation of sinusoidal capillaries in the diaphysis, and expansion of the vascular area in bone, visualized by immunostaining of the sialoglycoprotein Endomucin (Emcn) (Figures 1A–1D and S1A–S1C). Irradiation also causes an increase in vessel permeability, as indicated by enhanced tracer extravasation (Figure S1C). Whereas CD31$^+$ Emcn$^-$ hematopoietic cells are largely absent after irradiation, endothelial CD31 expression is upregulated, and vessel-associated collagen IV$^+$ reticular fibers are disrupted (Figure 1C). At 1 day after irradiation, BM vascular morphology is already changed with higher expression of Emcn relative to 3 h post-irradiation (Figure S1D). At 4 days post-irradiation, alterations in vascular morphology, such as vessel dilation, are more profound, indicating dynamic changes over several days (Figure S1D). To reveal the morphological changes of ECs at single-cell level, we treated *Cdh5(PAC)-CreERT2 Rosa26-mTmG* double-transgenic mice (Table S1) with low doses of tamoxifen. The analysis of rare recombined and therefore isolated GFP$^+$ cells indicates substantial changes in EC size and shape complexity at single-cell resolution (Figures 1E and 1F). Next, we checked the density of ECs after irradiation, which was aided by *Cdh5(PAC)-mtdTomato-nGFP* (*Cdh5-mTnG*) reporter mice in which membrane-anchored tdTomato fluorescent protein labels the surface and histone H2B-coupled GFP (nGFP) the nuclei of ECs (Jeong et al., 2017) (Table S1). Confirming the specificity of this reporter, H2B-GFP signal co-localizes with nuclear ERG, a transcription factor and EC marker, in postnatal day (P) 6 heart endothelium but not in the EC-derived mesenchymal cell in heart valves (Figure S1E). Further proving that *Cdh5-mTnG* reporter marks genuine ECs but not EC-derived cell populations, GFP signal in bone decorates Emcn$^+$ and VEGFR2$^+$ (vascular endothelial growth factor receptor 2$^+$) ECs without labeling CD31$^+$ Emcn$^-$, B220$^+$, and lineage committed hematopoietic cells (Figures S1F–S1J). Lethal irradiation of adult *Cdh5-mTnG* mice revealed a significant increase in EC density and percentage both by analysis of bone sections and flow cytometry (Figures 1G and 1H). Moreover, a higher number and ratio of GFP$^+$EdU$^+$ signals are detected in *Cdh5-mTnG* bone sections after irradiation (Figure S1K). In contrast, active caspase 3 immunostaining and annexin V binding, which indicate apoptosis, are not increased in bone ECs at 3 or 24 h post-irradiation (Figures S1L and S1M). These results show that irradiation disrupts the normal organization of bone capillaries and leads to increases in EC density and vascular permeability.

To investigate whether irradiation disrupts the vasculature in other organs, we analyzed different vascular networks in *Cdh5-mTnG* mice. Strikingly, no overt changes in vessel morphology and EC density were visible in retina, heart, skin, and small intestinal villi, which have no extramedullary hematopoietic function (Figure S1N–S1Q). In spleen, a major adult extramedullary organ, lethal irradiation disrupts the white pulp and leads to significant higher density of splenic vessels (Figure 1I). These findings support that ECs are far more resistant to irradiation than hematopoietic cells and suggest that vascular alterations after irradiation are particularly strong in organs with hematopoietic function. Very similar to irradiation, the chemotherapy drug 5-fluoracil (5-FU) (Noach et al., 2003) induces profound changes in the bone vasculature including expansion of the Emcn$^+$ area and dilation of sinusoidal vessels, disruption of collagen IV$^+$ reticular fibers, CD31 upregulation in ECs, morphological alterations of ECs at the single-cell level, and increased EC density (Figures S2A–S2H).

To identify molecular changes in the bone endothelium after irradiation, we used fluorescence-activated cell sorting (FACS) to isolate GFP$^+$ ECs from adult (8–12 weeks old) *Cdh5-mTnG* long bone for RNA-seq analysis. These FACS-sorted GFP$^+$ cells show significant enrichment of core EC markers, confirming their endothelial identity (Figure 2A). Principal-component analysis (PCA) divides normal (control) GFP$^+$ ECs and irradiated GFP$^+$ ECs (7 days post-irradiation) into two separate clusters, both of which are distinct from other BM cell groups (Figure 2B). According to unsupervised clustering, normal ECs and irradiated ECs are more similar to hematopoietic cells than to bone mesenchymal cell populations (Figure 2C). Furthermore, we found that the endothelial transcriptome is significantly changed only 1 day after irradiation (Figures 2D and 2E). EC transcriptomes at 1 day and 7 days post-irradiation are also significantly different from each other, suggesting dynamic changes consistent with the structural alterations in the bone vasculature at different time points after the treatment (Figures 2D, 2E, and S1B–S1D). At 7 days after irradiation, GFP$^+$ bone ECs show profound changes in their transcription profile with more than 2,000 upregulated genes and downregulated genes at $p < 0.05$ significance level relative to control GFP$^+$ ECs (Figures 2F, 2G, and S2I). More than 4,000 differentially expressed genes were also detected between 1 and 7 days after irradiation (Figure 2H). Several molecular signals associated with vascular niche function are significantly changed in ECs exposed to irradiation (Figure 2I), whereas genes related to DNA damage and senescence are not significantly altered (Figures S2J and S2K). These data indicate that irradiation substantially changes the transcription profile of bone ECs, including genes associated with EC niche function.

Loss of Hematopoietic Cells Phenocopies Irradiation-Induced Vascular Defects

Irradiation and 5-FU treatment target multiple cell types (Maxwell et al., 2003; Yahyapour et al., 2018). As BM hematopoietic cells

(G) Nuclear GFP$^+$ (nGFP$^+$) ECs in control and irradiated *Cdh5-mTnG* diaphysis. Graph shows quantitation of GFP$^+$ cells (n = 6 in each group).
(H) FACS plot of GFP$^+$ cells from control and irradiated *Cdh5-mTnG* mice. Graph show frequency of GFP$^+$ cells (n = 20 in each group).
(I) Tile scan overview images and selected maximum intensity projections of spleen vessels in *Cdh5-mTnG* mice. Quantification of GFP$^+$ nuclei in each image field (Ctrl n = 6; 9 Gy n = 4) is shown.
Error bars, mean ± SEM. p values, two-tailed unpaired Student's t test.
See also Figure S1.

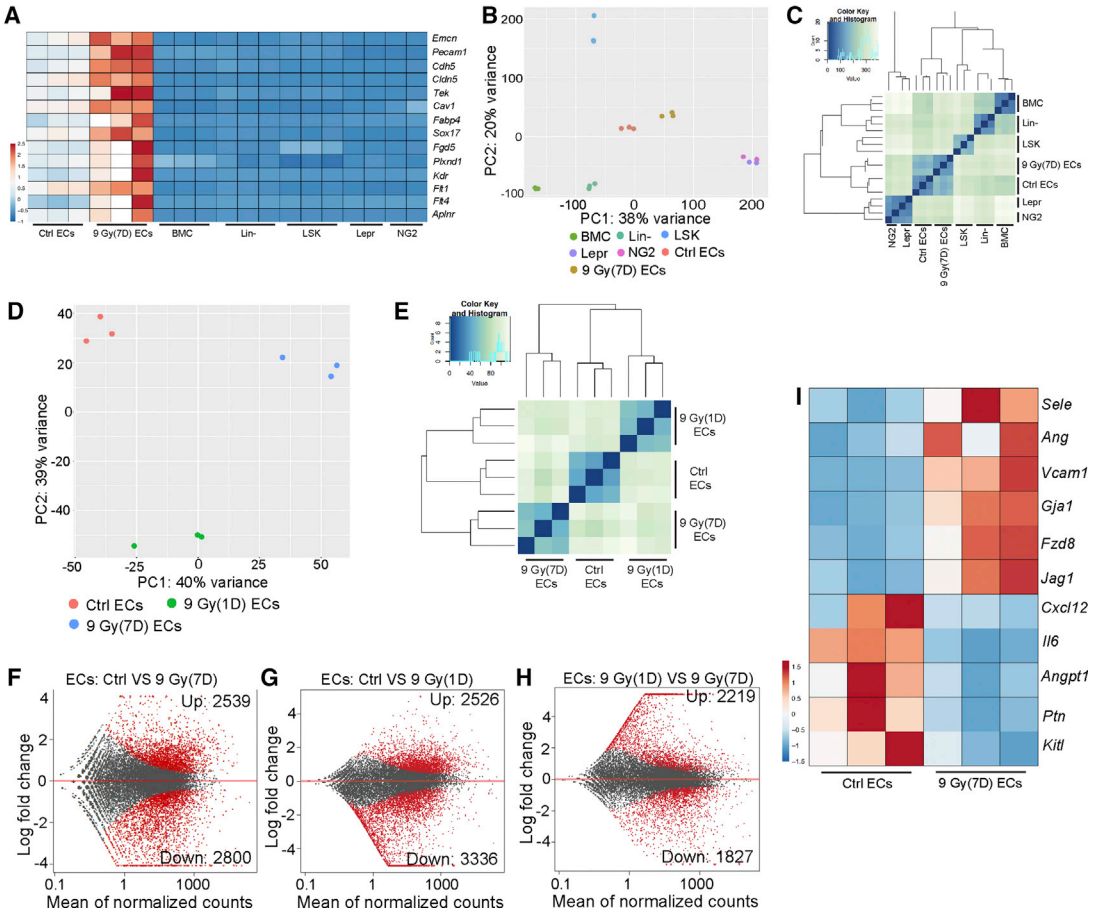

Figure 2. Irradiation Induces Dynamic Changes in the Transcription Profile of BM ECs

(A) Heatmap of selected EC-enriched genes in BM cells, Lin$^-$ cells, LSK cells, ECs, irradiated ECs (9 Gy, 7 days), Lepr$^+$, and NG2$^+$ cells.

(B) PCA plot of control and irradiated ECs together with other BM cell types. Data for Lepr$^+$ and NG2$^+$ cells were previously published (Asada et al., 2017).

(C) Sample distance analysis of different BM cell types, as indicated.

(D and E) PCA plot (D) and sample distance analysis (E) of ctrl ECs and ECs at 1 day or 7 days after irradiation.

(F–H) MA plot showing differentially expressed genes (red dots) between Ctrl ECs and ECs at 7 days after irradiation (9 Gy) (F), Ctrl ECs and ECs at 1 day after irradiation (G), and ECs at 1 and 7 days after irradiation (H), as indicated.

(I) Heatmap of selected HSC niche-related genes after irradiation.

See also Figure S2.

are largely eliminated after irradiation and chemotherapy, we reasoned that this loss might be a key contributor to the observed vascular defects. To test this hypothesis, we generated *Vav1-Cre Rosa26-DTR* mice (*DTR*$^{i\Delta HC}$) expressing diphtheria toxin receptor in hematopoietic cells (Table S1). The *Vav1-Cre* line used in these experiments does not induce recombination in ECs in adult femur (Figures S3A–S3D). Moreover, diphtheria toxin injection into *Vav1-Cre* Cre-negative mice has no effect on hematopoietic cells and bone vessels (Figure S3E). In contrast, diphtheria toxin injection in *DTR*$^{i\Delta HC}$ animals results in significant deletion of hematopoietic cells including Lin$^-$ Sca1$^+$ cKit$^+$ (LSK) multipotent progenitors (Figures 3A, 3F, S3F, and S3G). This hematopoietic cell ablation model, which is independent of irradiation and chemotherapy, leads to expansion of the Emcn$^+$ area, dilation of sinusoidal vessels, higher EC density, morphological alterations of BM ECs, disruption of reticular fibers, and increased permeability (Figures 3B–3F), phenocopying the vascular alterations after irradiation and 5-FU treatment. Furthermore, RNA-seq analysis of sorted *DTR*$^{i\Delta HC}$ ECs reveals similar changes in niche-related gene transcripts (Figures S3H–S3J). These data indicate that hematopoietic cells maintain physiological properties of the bone vasculature and suggest the existence of reciprocal interactions between hematopoietic cells and ECs.

Transplantation of the same number of different hematopoietic cell subpopulations after irradiation showed that non-committed, lineage-negative cells (Lin$^-$: Ter119$^-$ CD5$^-$ CD11b$^-$ CD45R$^-$ Ly-6G/C$^-$) induce vessel regeneration more efficiently than lineage committed cells (Lin$^+$) (Figures 3G and S3K). Multipotent progenitor LSK cells are even more efficient in this assay and induce vessel regeneration within 16 days even when a lower number of cells was transplanted (Figures 3H, 3I, and S3L). Following the transplantation of LSK cells, recovering BM vessels show improved vessel integrity and a reduction of the Emcn$^+$ area, indicating reduced vessel dilation (Figures 3H and 3I). BM regeneration after irradiation and transplantation does

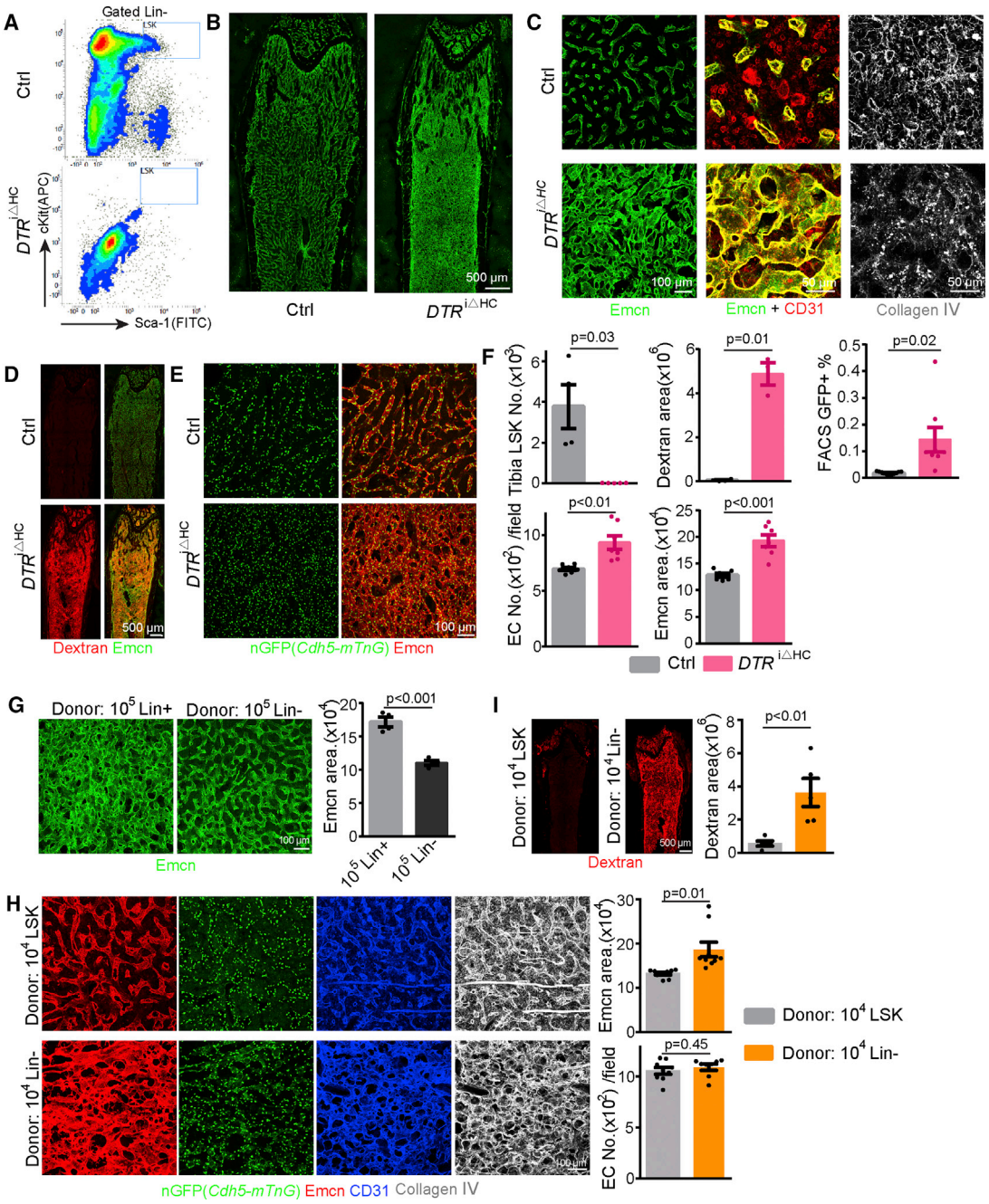

Figure 3. Diphtheria Toxin-Mediated Hematopoietic Cell Ablation Mimics Irradiation-Induced Vascular Defects

(A) FACS plot of LSK cells 4 days after diphtheria toxin injection in *DTR*$^{i\Delta HC}$ and control mice.

(B) Tile scan overview images of Emcn-stained vessels in DTA-treated control and *DTR*$^{i\Delta HC}$ long bone.

(C) High-magnification images showing Emcn, CD31, and collagen IV immunostaining in *DTR*$^{i\Delta HC}$ and control femur.

(D) Tile scan images showing extravasation of fluorescent Dextran in *DTR*$^{i\Delta HC}$ and control long bone.

(E) *Cdh5-mTnG*–controlled GFP$^+$ EC nuclei and Emcn staining in *DTR*$^{i\Delta HC}$ and control diaphysis.

(F) Quantification of LSK cell number (Ctrl = 4, *DTR*$^{i\Delta HC}$ = 5), Emcn$^+$ area (Ctrl = 7, *DTR*$^{i\Delta HC}$ = 7), Dextran$^+$ area (Ctrl = 4, *DTR*$^{i\Delta HC}$ = 3), and GFP$^+$ cells per image (Ctrl = 7, *DTR*$^{i\Delta HC}$ = 7, frequency of GFP$^+$ cells by FACS (Ctrl = 11, *DTR*$^{i\Delta HC}$ = 8).

(G) Representative images and quantification of Emcn$^+$ area at 16 days after irradiation and transplantation of 4 × 10^5 Lin$^-$ or Lin$^+$ cells (n = 4 in each group)

(H) Emcn, GFP$^+$ EC nuclei, CD31, and collagen IV at 16 days after irradiation and transplantation of 2 × 10^4 Lin$^-$ or LSK cells. Quantification of Emcn area (LSK = 10, Lin$^-$ = 9) and GFP$^+$ EC nuclei in each image field (LSK = 9, Lin$^-$ = 8).

(I) Tile scan overview images showing Dextran extravasation at 16 days after irradiation and transplantation of 2 × 10^4 Lin$^-$ or LSK cells. Quantification of Dextran$^+$ area (LSK = 5, Lin$^-$ = 5).

Error bars, mean ± SEM. p values, two-tailed unpaired Student's t test. See also Figure S3.

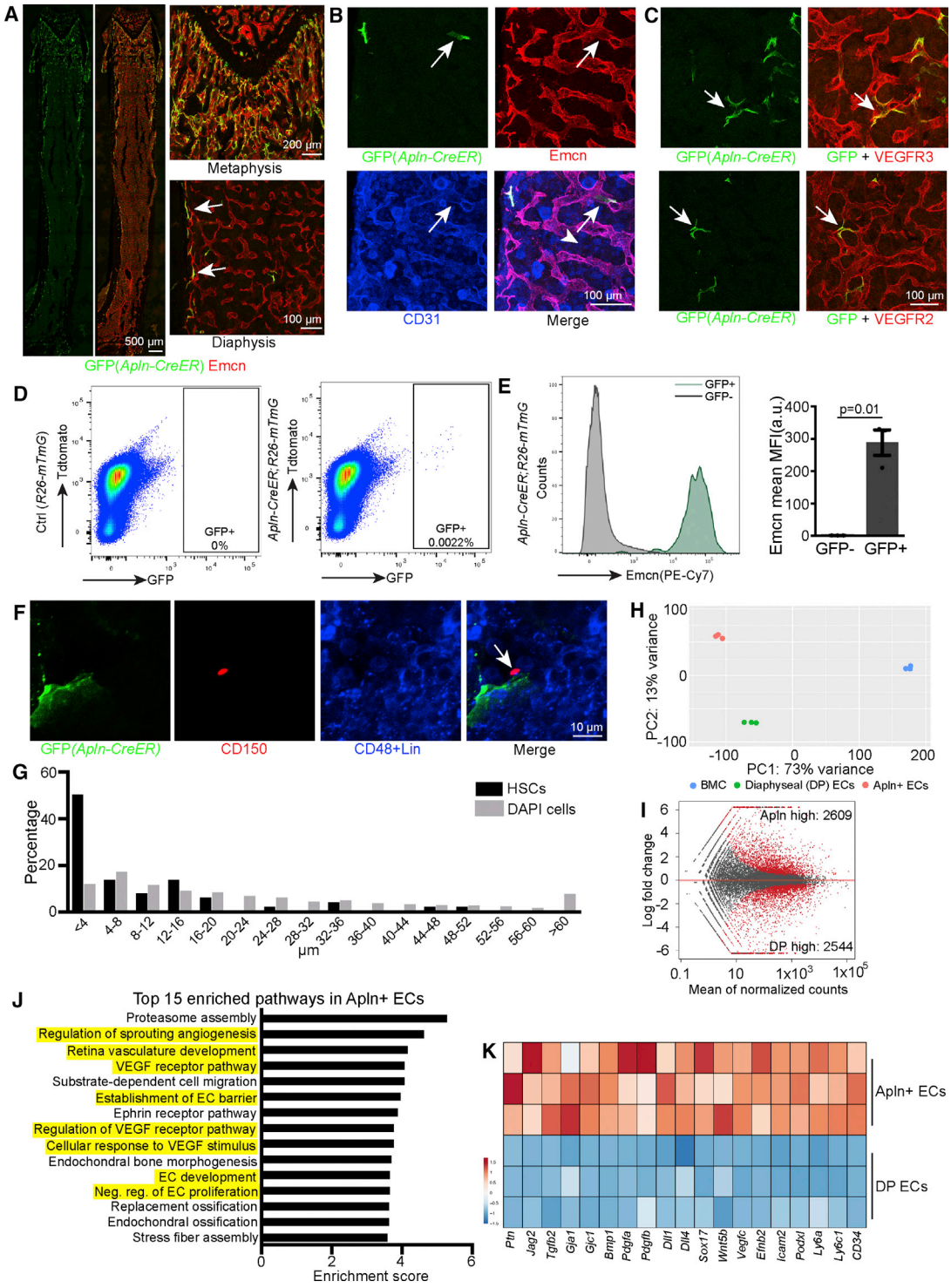

Figure 4. Identification of Apln$^+$ ECs in Adult BM

(A) Confocal tile scan images (left) showing distribution of GFP$^+$ cells in *Apln-mTmG* mice. High magnifications (right) show enlarged regions of the metaphysis and diaphysis. Arrows mark GFP$^+$ cells in endosteum.

(B and C) Emcn and CD31 (B) and VEGFR2 and VEGFR3 (C) staining in adult *Apln-mTmG* femur. Arrows mark GFP$^+$ ECs.

(D) FACS plots of GFP$^+$ cells isolated from *Apln-mTmG* mice.

(E) Histogram of Emcn expression in GFP$^-$ and GFP$^+$ cells. Quantification of mean fluorescence intensity (MFI) in GFP$^-$ and GFP$^+$ cells (n = 3 per group). Error bars, mean ± SEM. p values, two-tailed unpaired Students' t test.

(F) CD150$^+$ Lin$^-$ CD48$^-$ HSC (arrow) and GFP$^+$ EC in the metaphysis and metaphysis-diaphysis transition area of *Apln-mTmG* mice.

(legend continued on next page)

not involve the differentiation of donor-derived LSK cells into ECs in the recipient vasculature (Figures S3N and S3O). Mathematical regression analysis indicates that the number of BM nuclear cells (BMNCs) in a broad range (2×10^6 to 8×10^6 cells) is not proportional to the extent of vessel regeneration (Figures S3M, S7L, and S7Q). These data argue that LSK cells, which are enriched in hematopoietic stem and progenitor cells (HSPCs), have specific properties that promote the recovery of the recipient vasculature after irradiation more efficiently than other hematopoietic cell subsets.

Identification of Apln$^+$ ECs in Adult BM

Whereas different EC subpopulations have been proposed to provide vascular niches for HSPCs in BM, it is currently unknown whether the recovery of the bone vasculature after irradiation or 5-FU treatment is mediated by all or only certain ECs. *Bmx-CreERT2* transgenic mice enable efficient and irreversible genetic labeling of arterial ECs (Ehling et al., 2013; Xu et al., 2018). To check whether arterial cells contribute to bone vessel regeneration, we generated *Bmx-CreERT2 Rosa26-mTmG* (*Bmx-mTmG*) double-transgenic mice in which tamoxifen injection irreversibly labels arterial ECs and their descendants by GFP expression (Table S1). Irradiation and 5-FU treatment did not induce significant morphological changes of arteries (Figures S4A, S4B, and S2F). *Bmx-CreERT2* mice mediated lineage tracing indicates no apparent contribution of arterial ECs to regenerating sinusoidal vessels after irradiation and BM transplantation (Figure S4C) (Ehling et al., 2013; Xu et al., 2018).

Apelin (Apln) is a peptide ligand secreted by a subpopulation of angiogenic ECs in different growing and regenerating organs (Tian et al., 2013). To analyze the distribution of Apln$^+$ ECs in adult bone, we generated adult *Apln-CreER Rosa26-mTmG* (*Apln-mTmG*) mice and tracked the GFP-labeled ECs shortly (2 days) after tamoxifen injection (Table S1). *Apln-CreER*-labeled cells were predominantly found in the metaphysis, endosteum, and the transition area between the metaphysis and diaphysis (Figure 4A). GFP$^+$ cells express Emcn, CD31, VEGFR2, VEGFR3, and VE-cadherin confirming their endothelial identity (Figures 4B, 4C, and S4H). Apln$^+$ ECs express Sca-1 but are, unlike arterial ECs, not covered by αSMA$^+$ vascular smooth muscle cells (vSMCs) (Figure S4I). FACS-isolated *Apln-CreER*-labeled ECs represent about 0.0032% ± 0.0003% of total BM cells and 12.4% ± 1.3% of bone ECs (Figures 4D and 4E). Strikingly, Apln$^+$ EC are closely associated with a subset of CD150$^+$ CD48$^-$ Lin$^-$ HSCs that are located in the metaphysis and the transition zone between the metaphyseal and diaphyseal vasculature (Figures 4F and 4G). To understand whether Apln$^+$ ECs are similar to other BM ECs, we isolated *Apln-CreER*-labeled (GFP$^+$) cells from *Apln-mTmG* mice by FACS for RNA-seq analysis. These cells were compared to ECs from the *Cdh5-mTnG* diaphysis (Figure S4D). Confirming their endothelial identity, both sorted cell populations show significantly higher expression of EC markers relative to other BM cells, but they also show substantial differences in gene expression and form separate clusters in principal components analysis (Figures 4H and S4E). While 2,609 genes are significantly enriched in Apln$^+$ ECs, 2,544 genes show significantly higher expression in the diaphyseal endothelium (Figures 4I and S4F). Based on Gene Ontology (GO) biological process analysis, most of the 15 top enriched pathways in Apln$^+$ ECs are related to angiogenesis and, in particular, vascular endothelial growth factor (VEGF) signaling (Figure 4J). In contrast, pathways enriched in diaphyseal ECs relate to leukocyte adhesion, tethering and rolling, which is consistent with the known function of sinusoidal vessels in the trafficking of hematopoietic cells (Figure S4G). Accordingly, numerous mRNAs associated with HSC niche function of the endothelium, such as *Ptn* (encoding Pleiotrophin), gap-junction proteins, and Notch ligands are substantially higher in Apln$^+$ ECs (Figure 4K) (Guo et al., 2017; Himburg et al., 2010; Taniguchi Ishikawa et al., 2012; Tikhonova et al., 2019), suggesting that Apln$^+$ ECs may potentially play a role in hematopoiesis. In addition, Apln$^+$ ECs have special molecular properties and show expression of certain arterial markers, such as *Dll4* (Delta-like 4), *Efnb2* (ephrin-B2), *Ly6a* (Sca-1), *Gja1* (connexin 43), *Cav1* (caveolin-1), and the transcription factor *Sox17*, even though they are not typical arterial cells based on their localization and the lack of αSMA$^+$ cell coverage (Figures 4K, S4E, and S4I). These data indicate that Apln$^+$ ECs in adult bone represent a specialized endothelial subpopulation.

Apln$^+$ ECs Regulate Steady-State Hematopoiesis

To investigate the function of Apln$^+$ ECs, we generated *Apln-CreER Rosa26-DTA* (*DTA*$^{i\Delta Apln}$) mice enabling tamoxifen-induced elimination of Apln$^+$ ECs (Figure S4M). This procedure damages metaphyseal vessels in direct proximity of the growth plate, results in slight dilation of sinusoidal vessels in the diaphysis, and increases the permeability of the bone vasculature (Figures S4N and S4O). Notably, vascular defects in the *DTA*$^{i\Delta Apln}$ model are morphologically distinct from the damage seen after myeloablative treatments, namely, irradiation, 5-FU, or the *DTR*$^{i\Delta HC}$ model (Figures S4N, 1B, 1C, S2B, 3B, and 3C). Based on flow cytometric analysis, the ablation of Apln$^+$ ECs leads to profound reductions in the percentage and absolute number of LSK cells and HSCs (Figures 5A and 5B). The remaining CD150$^+$ CD48$^-$ Lin$^-$ HSCs are found in larger distance from BM vessels in *DTA*$^{i\Delta Apln}$ mice (Figure 5C). Depletion of long-term HSCs in *DTA*$^{i\Delta Apln}$ bone was confirmed by CD45.1/CD45.2 long-term competitive repopulation experiments (Figures 5D and S5A). We also detected a significant decrease of common lymphoid progenitors and common myeloid progenitors (Figure 5B), indicating that Apln$^+$ ECs are required for the maintenance of both multipotent and

(G) Distribution of distance between DAPI$^+$ cells (n = 3,872) or CD150$^+$ Lin$^-$ CD48$^-$ HSCs (n = 52) and GFP$^+$ ECs cells in the metaphysis and metaphysis-diaphysis transition area of *Apln-mTmG* mice.
(H) PCA plot of total BM cells (BMC), Apln$^+$ ECs (from whole bone), and diaphyseal ECs (DP ECs).
(I) MA plot showing differentially expressed genes between Apln$^+$ ECs and DP ECs.
(J) Top 15 enriched pathways in GO analysis in Apln$^+$ ECs relative to DP ECs.
(K) Heatmap of selected genes in Apln$^+$ ECs.
See also Figure S4.

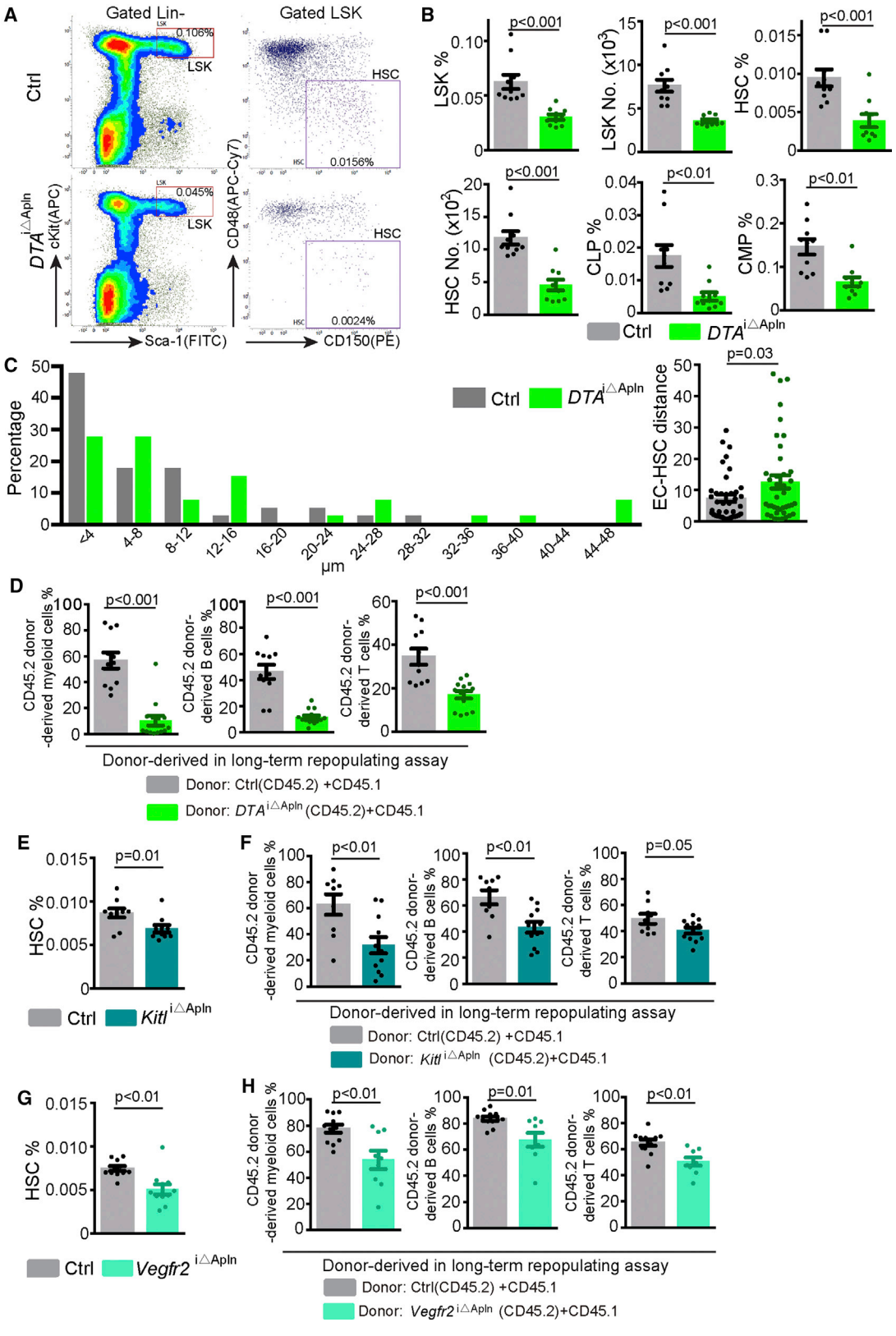

(legend on next page)

oligopotent HSPCs. The number of BMNCs is not significantly altered, whereas the percentage of B lymphocytes decreases significantly in *DTA*$^{i\Delta Apln}$ bone (Figure S5B). In contrast, the percentages of CD45$^-$ Ter119$^-$ CD31$^-$ CD51$^+$ CD140a$^+$ and of CD45$^-$ Ter119$^-$ CD31$^-$ Lepr$^+$ CD140b$^+$ perivascular cells are not changed significantly (Figure S5C). Peripheral blood (PB) count results show a significant decrease of lymphocyte and increase in the percentage of granulocytes in *DTA*$^{i\Delta Apln}$ mice relative to control (Figure S5D). FACS analysis indicates a significantly higher percentage of myeloid cells in *DTA*$^{i\Delta Apln}$ PB, whereas the percentage of total CD45$^+$ leukocytes is not significantly changed (Figure S5E). Moreover, certain proinflammatory cytokines, in particular, interleukin (IL)-1α and IL-6, are elevated in blood plasma of *DTA*$^{i\Delta Apln}$ mice (Figure S5F). The percentage change of myeloid cells and B lymphocyte are also seen in liver but not spleen of *DTA*$^{i\Delta Apln}$ mice (Figures S5G and S5H). These results indicate that Apln$^+$ ECs help to maintain a normal, non-inflammatory milieu and play a critical role in steady-state hematopoiesis.

Stem cell factor (SCF, encoded by the gene *Kitl* in mice) is an essential regulator of HSC self-renewal and function (Asada et al., 2017; Comazzetto et al., 2019; Ding et al., 2012; Xu et al., 2018). *Apln-CreER*-mediated inactivation of the *Kitl* gene causes a significantly lower percentage of HSCs in the BM of the resulting *Kitl*$^{i\Delta Apln}$ mutants relative to littermate controls (Figure 5E). This reduction of HSCs in *Kitl*$^{i\Delta Apln}$ mice is confirmed by CD45.1/CD45.2 long-term competitive repopulating assay (Figure 5F), whereas the PB count in *Kitl*$^{i\Delta Apln}$ mice is normal (Figure S5I). In Apln$^+$ ECs, genetic inactivation of VEGF receptor 2 (*Vegfr2*$^{i\Delta Apln}$), which is the major receptor of VEGF-A, also causes a significant reduction in HSC percentage (Figures 5G, 5H, and S5J). These results indicate that Apln$^+$ ECs and signaling processes in these cells are necessary for HSC maintenance.

Apln-CreER mice have been generated by a knockin of tamoxifen-inducible CreER into the X-linked *Apln* locus (Tian et al., 2013), which disrupts the function of the gene globally so that *Apln-CreER* hemizygous male mice (T/y) are null mutants lacking the ability to generate apelin peptide. Excluding the possibility that the defects in *Apln-CreER* males are caused by lost *Apln* function, hematopoiesis and hematopoietic reconstitution are comparable for *Apln-CreER* hemizygous (T/y) and littermate wild-type (+/y) male mice in the absence of tamoxifen treatment (Figures S5K and S5L). Together, these results indicate that a small subpopulation of Apln$^+$ ECs but not apelin expression is required for steady-state hematopoiesis and HSC maintenance.

Role of Apln$^+$ ECs in BM Transplantation and Vascular Regeneration

To investigate potential functional roles of Apln$^+$ ECs in hematopoietic reconstitution, we transplanted BM cells into *DTA*$^{i\Delta Apln}$ and littermate control recipients. Transplantation of genetically labeled (GFP$^+$) BM cells from *Vav1-Cre Rosa26-mTmG* donors and immunostaining of bone sections and quantitative FACS suggested limited engraftment and expansion of transplanted hematopoietic cells in BM of *DTA*$^{i\Delta Apln}$ recipients at 5 days after lethal irradiation, indicating that Apln$^+$ ECs are necessary for efficient transplantation (Figures 6A–6D). To understand how Apln$^+$ ECs contribute to hematopoietic reconstitution, we performed lineage tracing experiments. Adult *Apln-mTmG* were treated with 4-hydroxytamoxifen (4-OHT) at 1 day before lethal irradiation and transplantation, whereas control *Apln-mTmG* mice received the same dosage of 4-OHT without irradiation. In these latter animals, the distribution of *Apln-CreER*-labeled ECs is not substantially changed between 1 and 22 days after 4-OHT administration (Figures 6E and 4A). In contrast, irradiated *Apln-mTmG* mice show a profound increase of GFP$^+$ cells in the diaphyseal vasculature, indicating that the regeneration of bone vessels involves the expansion of Apln$^+$ ECs into the diaphyseal (i.e., sinusoidal) vascular network (Figure 6E). Irradiation without transplantation can trigger similar expansion of Apln$^+$ ECs, indicating that this process does not require allogenic BM transplantation (Figure S6D). The descendant cells generated by the expansion of Apln$^+$ ECs are reduced but do not regress completely after stable engraftment of the transplanted hematopoietic cells (Figure S6E). The progeny of Apln$^+$ ECs includes cells that are covered by αSMA$^+$ vSMCs, suggesting adult Apln$^+$ ECs have the potential to generate arterial ECs in response to irradiation stress (Figure S6F). Together, these results indicate that Apln$^+$ ECs contribute to allogenic transplantation and actively participate in the remodeling of the BM vasculature after irradiation.

We also investigated another subpopulation of BM ECs, namely, Esm1$^+$ ECs, which were genetically labeled in *Esm1-CreER R26-mTmG* mice (Figure S6G) (Pitulescu et al., 2017; Rocha et al., 2014). Esm1$^+$ ECs and Apln$^+$ ECs show similar labeling percentages in the diaphysis under steady-state conditions (Figure S6G). In contrast to Apln$^+$ ECs, genetic ablation experiments with *Esm1-CreER R26-DTA* mice (*DTA*$^{i\Delta Esm1}$) (Figures S6H and S6L) fail to influence the percentage of HSCs, BM hematopoietic cell composition, PB composition under steady-state conditions (Figures S6H–S6K), and transplantation efficiency (Figures 6F and S6L–S6M). Moreover, Esm1$^+$ ECs are not preferentially located in the metaphysis and endosteum and fail to expand

Figure 5. Apln$^+$ ECs Regulate HSC Maintenance and Steady-State Hematopoiesis

(A) FACS plot of LSK cells and HSCs in control and *DTA*$^{i\Delta Apln}$ mice. Numbers in boxes represent the percentage of the cell population among all BM cells.

(B) Quantification of the number and percentage of LSK cells, HSCs, and oligopotent progenitor cells in control (n = 10) and *DTA*$^{i\Delta Apln}$ (n = 10) mice. CLP, common lymphoid progenitor; CMP, common myeloid progenitor.

(C) Quantitative distribution of distance between CD150$^+$CD48-Lin$^-$ HSCs and vessels in whole BM of control (n = 40 HSC from 4 mice) and *DTA* $^{i\Delta Apln}$ mice (n = 40 HSC from 5 mice).

(D) Long-term competitive repopulation assay showing donor-derived (CD45.2, control = 11 and *DTA*$^{i\Delta Apln}$ = 14) myeloid cells, B cells, and T cells.

(E) Percentage of BM HSCs in control (n = 10) and *Kitl* $^{i\Delta Apln}$ mice (n = 10).

(F) Long-term competitive repopulation assay showing donor-derived (CD45.2, control = 9 and *Kitl*$^{i\Delta Apln}$ = 12) myeloid cells, B cells, and T cells.

(G) Percentage of BM HSCs in control (n = 11) and *Vegfr2* $^{i\Delta Apln}$ mice (n = 11).

(H) Long-term competitive repopulating assay showing donor-derived (CD45.2, control = 12 and *Vegfr2*$^{i\Delta Apln}$ = 9) myeloid cells, B cells, and T cells.

Error bars, mean ± SEM. p values, two-tailed unpaired Student's t test. See also Figure S5.

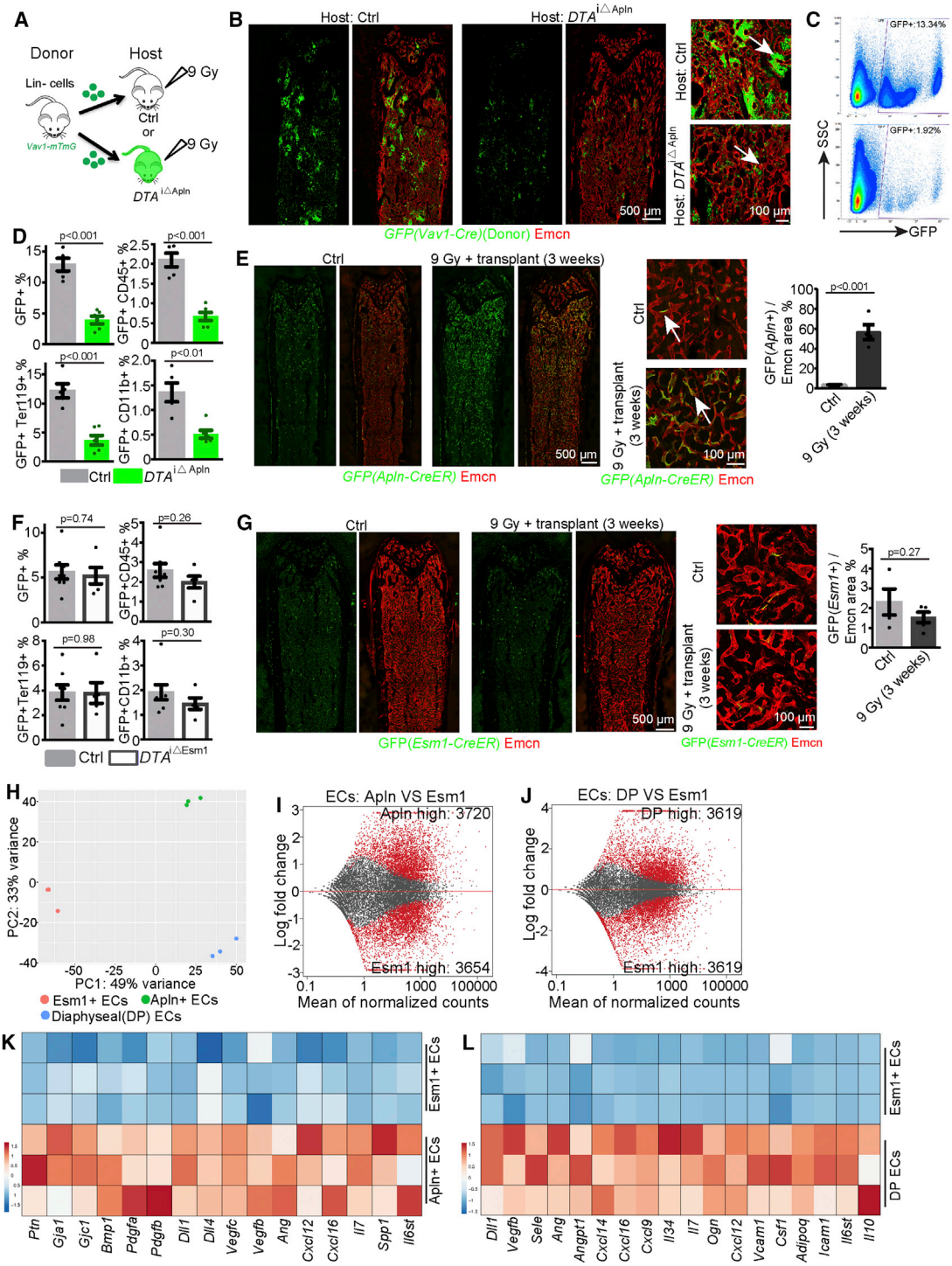

Figure 6. Apln$^+$ ECs Are Necessary for BM Transplantation

(A) Transplantation of cells from *Vav1-Cre R26-mTmG* mice into Ctrl and *DTA*$^{i\Delta Apln}$ hosts.

(B) Tile scan overview images and selected maximum intensity projections of control and *DTA*$^{i\Delta Apln}$ bone 5 days after irradiation and transplantation with 3×10^5 *Vav1-Cre R26-mTmG* Lin$^-$ cells. Arrows indicate donor-derived GFP$^+$ cells.

(C) FACS plots of GFP$^+$ cells from control and *DTA* $^{i\Delta Apln}$ host BM.

(D) Quantification of GFP$^+$, GFP$^+$CD45$^+$, GFP$^+$Ter119$^+$, and GFP$^+$CD11b$^+$ cells in control (n = 5) and *DTA* $^{i\Delta Apln}$ (n = 6) host BM.

(E) Tile scan overview images and selected maximum intensity projections showing lineage tracing of GFP$^+$ cells in *Apln-mTmG* long bone with or without irradiation and transplantation. Arrows mark GFP$^+$ Emcn$^+$ ECs. Quantification of GFP$^+$ area relative to Emcn$^+$ area in diaphysis (n = 4 in each group).

(legend continued on next page)

after irradiation (Figure 6G). We used FACS to isolate Esm1$^+$ ECs (Figure S6N) for RNA-seq analysis. These cells show significant enrichment of core EC markers relative to hematopoietic cells and mesenchymal cells (Figure S6O) but are distinct from Apln$^+$ ECs and total diaphyseal ECs (Figures 6H–6J and S6P). Remarkably, Esm1$^+$ ECs show low expression of a broad range of niche factors and angiocrine factors (Figures 6K and 6L), further arguing that this subpopulation of ECs is not critical for hematopoiesis and transplantation. These results show that not all BM ECs are equally important for HSCs maintenance, hematopoiesis, and transplantation. Moreover, the phenotype in *DTA*$^{i\Delta Apln}$ mutants is most probably induced by specific ablation of Apln$^+$ ECs and not by side effects of EC death or unspecific toxicity of diphtheria toxin.

Crosstalk between Apln$^+$ ECs and HSPC during BM Regeneration

The results above indicate that HSPC/LSK cells and Apln$^+$ ECs play critical roles after irradiation and transplantation (Figures 3G–3I and 6A–6E), which raises the question whether the activity of these cell populations is coupled during hematopoietic reconstitution and bone vessel regeneration. Analysis of RNA-seq results of LSK cells and Lin$^-$ HSPCs in combination with previously published data for Lepr$^+$ and NG2/Cspg4$^+$ perivascular niche cells (Asada et al., 2017) indicates that LSK cells are a major source of VEGF-A (encoded by the gene *Vegfa*) in BM (Figure S7A). Higher expression of VEGF-A protein in LSK cells is confirmed by ELISA (Figure S7B). Irradiation significantly disrupts autocrine expression of *Vegfa* by ECs, which, together with the loss of LSK cells, results in profoundly reduced *Vegfa* expression in total BM cells (Figures S7A–S7C). Previous work has shown that donor-cell-derived VEGF-A is necessary for transplantation (Gerber et al., 2002). This finding is confirmed by our own transplantation experiments with BM cells from *Vav1-Cre Vegfa* (*Vegfa*$^{\Delta HC}$) double-heterozygous mice into lethally irradiated recipients (Figures S7F–S7H) (Ferrara et al., 1996). However, it was unclear whether hematopoietic cells or ECs are the cellular target of VEGF-A, as both possibilities are favored by different reports (Gerber et al., 2002; Hooper et al., 2009). To address this question, we have combined inactivation the *Kdr* (*Vegfr2*) gene, which encodes the main receptor for VEGF-A, in different cells types. In BM transplantation experiments, donor cells from hematopoietic cell-specific *Vav1-Cre Vegfr2 (floxed/floxed)* (*Vegfr2*$^{\Delta HC}$) mutants and control animals do not lead to significant differences in transplantation efficiency or recipient BMNC number (Figures S7I–S7J). However, *Vegfr2*$^{\Delta HC}$ BM donor transplantation results in a significant increase of CD11b$^+$ myeloid cells relative to control BM (Figure S7J), indicating a role of VEGFR2 in hematopoietic cell differentiation.

Expression of *Vegfr2* is strongly increased in irradiated ECs (Figure S7D), and RNA-seq shows that VEGF signaling pathway components are enriched in Apln$^+$ ECs (Figures 4J and S7E). To test whether Apln$^+$ ECs might respond to VEGF-A from transplanted BM cells, we generated tamoxifen-induced adult *Apln-CreER Vegfr2 (floxed/floxed)* (*Vegfr2*$^{i\Delta Apln}$) mutants. Transplantation of Lin$^-$ HSPCs into lethally irradiated *Vegfr2*$^{i\Delta Apln}$ animals results in delayed bone vessel normalization, lower abundance of BMNCs, LSK cells, myeloid cells, and B cells, but not T cells, relative to littermate control recipients (Figures 7A, 7B, and S7K–S7M). In an independent approach, we performed transplantation experiments with pan-endothelial *Cdh5-CreERT2 Vegfr2 (floxed/floxed)* (*Vegfr2*$^{i\Delta EC}$) recipients (Figure S7N). Relative to littermate control recipients, lethally irradiated *Vegfr2*$^{i\Delta EC}$ mutants show impaired vascular regeneration, lower percentage of LSK cells, and fewer myeloid cells and B cells at 2.5 weeks after transplantation (Figure S7N).

Conversely, combining the transplantation of a limited number of 10^4 Lin$^-$ BM cells after lethal irradiation with intravenous administration of recombinant VEGF-A improves recipient survival, normalization of the BM vasculature, repopulation efficiency in primary transplantations, and significantly increases HSC frequency relative to vehicle-treated controls (Figures 7C–7F and S7O–S7R). To understand how VEGF-A improves transplantation efficiency, we administrated VEGF-A to *Apln-mTmG* mice together with tamoxifen. In these experiments, VEGF-A infusion significantly increases the percentage of Apln$^+$ ECs in diaphysis (Figure 7G). VEGF-A also significantly increases the transcription of *Apln* in cultured ECs *in vitro* (Figure 7H). Thus, VEGF-A can change the molecular properties of ECs in adult BM and endothelial *Apln* expression. Consistent with previous research (Gerber et al., 2002), VEGF-A has also direct effects on Lin$^-$ HSPCs and promotes the formation of leukocytes in methylcellulose assay *in vitro* (Figures 7I and S7S).

DISCUSSION

In this study, we provide new insight into the nature of irradiation-induced damage to the bone vasculature and the dynamic changes in BM vessels during regeneration and repopulation. Irradiation leads to vessel dilation, increased EC density, and vascular permeability, which are accompanied by changes in EC morphology and gene expression in bone. These vascular defects are phenocopied by a genetic model of hematopoietic cell ablation and are efficiently rescued by transplantation of multipotent LSK cells, which are a major source of VEGF-A. Furthermore, our work identifies a subpopulation of bone ECs, namely, Apln$^+$ ECs, as important regulators of HSC function and BM regeneration after transplantation. While previous work has already established that

(F) Quantitative analysis of transplantation efficiency in *DTA*$^{i\Delta Esm1}$ mice at 5 days after irradiation and transplantation of 10^5 Lin$^-$ cells from *Vav1-mTmG* mice (Ctrl = 8; *DTA* $^{i\Delta Esm1}$ = 5).

(G) Lineage tracing of GFP$^+$ cells in *Esm1-CreER R26-mTmG* mice with the same protocol as in (E). Quantification of GFP$^+$ area relative to Emcn$^+$ area in diaphysis (Ctrl = 4; 9 Gy = 5).

(H) PCA plot of Apln$^+$ ECs, Esm1$^+$ ECs, and total DP ECs under steady state.

(I and J) MA plot showing genes with differential expression between Esm1+ ECs and Apln+ ECs (I) and between Esm1+ ECs and total DP ECs (J).

(K and L) Heatmap showing expression of selected angiocrine or niche-related genes in Apln$^+$ ECs relative to Esm1$^+$ ECs (K), and in Esm1$^+$ ECs relative to total DP ECs (L).

Error bars, mean ± SEM. p values, two-tailed unpaired Student's t test. See also Figure S6.

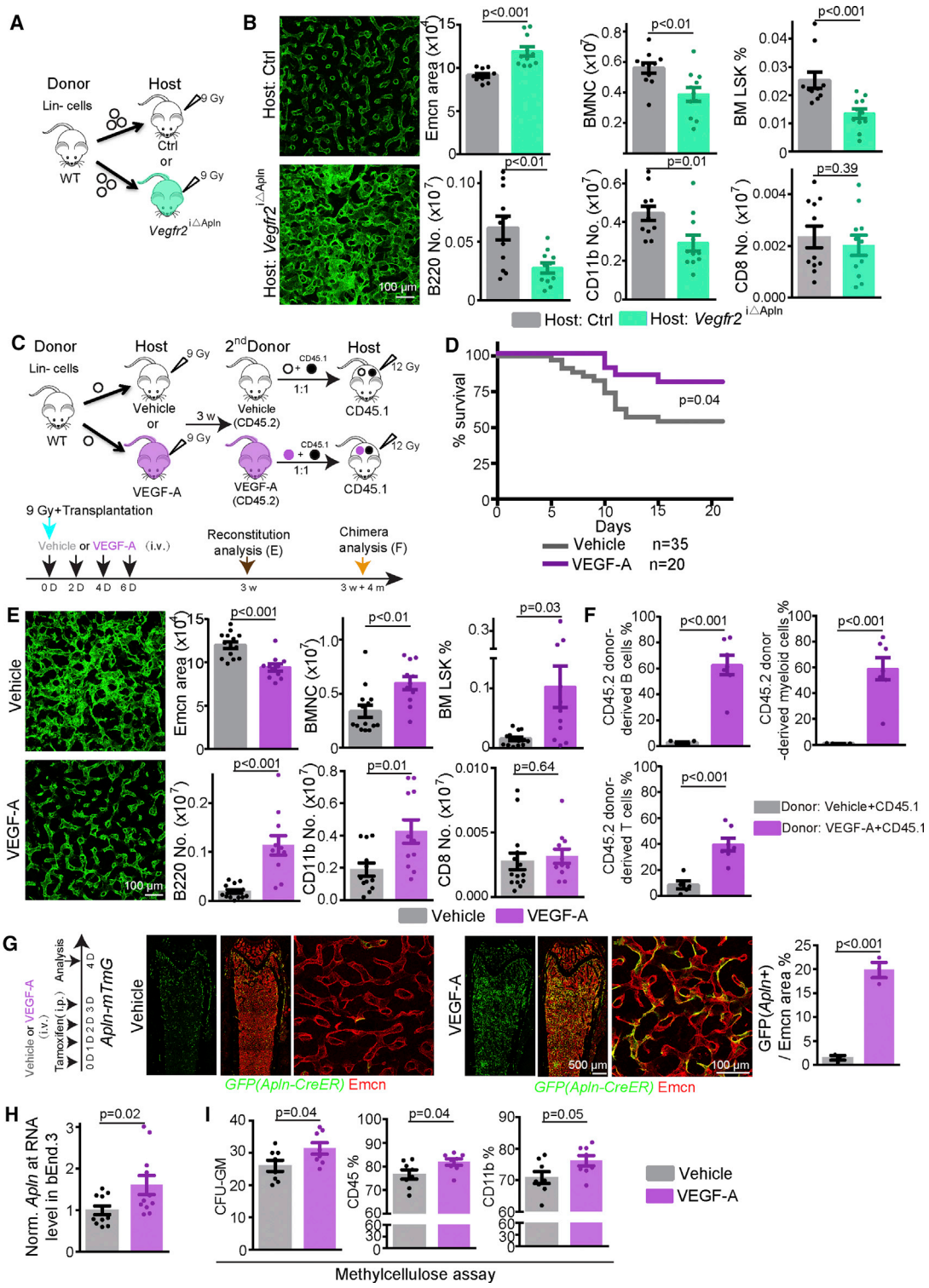

Figure 7. Crosstalk of HSPC with Apln$^+$ ECs in BM Vascular Regeneration and Hematopoietic Reconstitution

(A) Diagram depicting the transplantation of wild-type Lin$^-$ cells into Ctrl and *Vegfr2*$^{i\Delta Apln}$ host mice.

(B) Bone vessels at 2.5 weeks after transplantation in control or *Vegfr2*$^{i\Delta Apln}$ host mice. Quantification of Emcn$^+$ area, percentage of LSK cells, number of BMNCs, B220$^+$, CD11b$^+$, and CD8$^+$ cells in control (n = 10–11) and *Vegfr2* $^{i\Delta Apln}$ (n = 11) host mice.

(C) Scheme depicting VEGF-A treatment in combination with transplantation of wild-type Lin$^-$ cells.

(D) Survival curve of irradiated mice transplanted with 10^4 Lin$^-$ cells and intravenous injection of PBS (vehicle; n = 35) or recombinant VEGF-A (n = 20).

(legend continued on next page)

ECs and associated mesenchymal cells provide niches controlling HSC self-renewal and differentiation (Asada et al., 2017; Comazzetto et al., 2019; Ding et al., 2012; Méndez-Ferrer et al., 2010; Sugiyama et al., 2006; Tikhonova et al., 2019; Xu et al., 2018), we now assign critical functional properties to a small subset of Apln$^+$ ECs.

Our previous work has shown that neonatal Apln$^+$ ECs are enriched in CD31^{hi} Emcn^{hi} (type H and E) ECs, mediate postnatal osteogenesis, and generate other EC subtypes during development (Langen et al., 2017). The current study extends the function of Apln$^+$ ECs from osteogenesis to adult hematopoiesis and BM transplantation. Adult Apln$^+$ ECs express niche factors, such as connexin gap-junction proteins, Notch ligands, and pleiotrophin (PTN), that have been previously associated with HSPC function and BM reconstitution (Figure 4K). Expression of PTN, a secreted and matrix-binding growth factor, is increased in BM ECs after myelosuppressive irradiation and EC-specific inactivation of the murine *Ptn* gene impairs HSC regeneration (Himburg et al., 2010; Himburg et al., 2018). These results argue that adult Apln$^+$ ECs are an important source of niche factors.

Recent single-cell RNA-seq profiling classifies BM ECs into two groups of cells defined as Stab2^{high} ECs and Ly6a^{high} ECs, the latter includes 11% of total ECs (Tikhonova et al., 2019). Our own data show that Apln$^+$ ECs represent approximately 12% of total ECs, and Apln$^+$ ECs share a strikingly similar transcription profile with Ly6a^{high} ECs (Figure S4J), suggesting that these two subsets may be identical or overlapping entities. While other endothelial subpopulations, namely, Bmx$^+$ arterial ECs and Esm1$^+$ capillary ECs, show no appreciable expansion after irradiation, ECs derived from the Apln$^+$ population increase substantially in number and expand into the endothelium of the regenerating BM cavity. Hematopoietic reconstitution and vascular regeneration after irradiation are promoted by VEGF-A provided by transplanted BM cells and, in particular, by HSPCs and LSK cells, consistent with previous reports addressing the crucial role of the VEGF pathway in BM regeneration (Gerber et al., 2002; Hooper et al., 2009). Thus, regeneration of the vasculature during hematopoietic reconstitution involves reciprocal interactions between the transplanted BM cells and expanding, niche factor-providing Apln$^+$ ECs.

Apln$^+$ ECs may play an anti-inflammatory role required to maintain a balanced BM microenvironment. Apln$^+$ ECs show enriched expression of anti-inflammatory factors such as *Mmp*, *Tgfb2*, *Nos3*, and *Ptgis* (Aguirre et al., 2017; Bougaki et al., 2010; Jin et al., 2014; Manicone and McGuire, 2008; Dorris and Peebles, 2012; Knudsen et al., 1986). Accordingly, ablation of Apln$^+$ ECs leads to an increase of PB myeloid cells, which is a hallmark of numerous conditions with compromised BM function including aging, inflammation, or compromised stromal support (Kusumbe et al., 2016; Mann et al., 2018; Pietras, 2017; Tikhonova et al., 2019).

Based on the findings presented above, we propose that Apln$^+$ ECs in the adult skeletal system represent a population of specialized ECs, which are characterized by progenitor properties, are a source of niche factors, control multipotent, and oligopotent hematopoietic progenitors, and promote BM regeneration after myeloablative treatment. Our results provide insights into the cellular and molecular mechanisms controlling BM transplantation and highlight Apln$^+$ ECs as a potential therapeutic target in this process.

STAR★METHODS

Detailed methods are provided in the online version of this paper and include the following:

- KEY RESOURCES TABLE
- LEAD CONTACT AND MATERIALS AVAILABILITY
- EXPERIMENTAL MODEL AND SUBJECT DETAILS
- METHOD DETAILS
  - Cryosectioning, immunohistochemistry and permeability assays
  - Flow cytometry
  - Irradiation, transplantation, lineage separation and VEGF-A treatment
  - Blood count, blood plasma cytokine analysis and bone marrow cell number counting
  - ELISA
  - *In vitro* methycellulose and bEnd.3 assays
  - EdU incorporation
  - RNA extraction and quantitative PCR
  - RNA sequencing and data analysis
  - Confocal imaging and image processing
- QUANTIFICATION AND STATISTICAL ANALYSIS
- DATA AND CODE AVAILABILITY

SUPPLEMENTAL INFORMATION

Supplemental Information can be found online at https://doi.org/10.1016/j.stem.2019.10.006.

ACKNOWLEDGMENTS

Funding was provided by the Max Planck Society, the University of Münster, the Deutsche Forschungsgemeinschaft cluster of excellence "Cells in Motion", the European Research Council (AdG 339409 AngioBone; AdG 786672 PROVEC), and the Chinese Academy of Science. Y.L. was supported by Christiane Nüsslein-Volhard Stiftung.

(E) Bone vessels at 3 weeks after irradiation and treatment with vehicle (PBS + Lin$^-$ cells) or VEGF-A (VEGF-A + Lin$^-$ cells). Quantification of Emcn$^+$ area, percentage of LSK cells, number of BMNCs, B220$^+$, CD11b$^+$, and CD8$^+$ cells in vehicle (n = 12–14) and VEGF-A (n = 11)-treated mice.

(F) Secondary long-term competitive repopulating assay with donor-derived CD45.2 cells from 1st transplant of vehicle or VEGF-A-treated recipients. Graphs show percentage of CD45.2 donor-derived myeloid cells, B cells, and T cells (vehicle = 5, VEGF-A = 7).

(G) Confocal tile scan overview and high-magnification images of GFP and Emcn signals in the *Apln-mTmG* diaphysis after infusion of vehicle or VEGF-A. Quantification of GFP$^+$ cell relative to Emcn$^+$ (vehicle = 3, VEGF-A = 3).

(H) *Apln* transcripts in cultured bEnd.3 cells. *Actb* was used as control (vehicle = 11, VEGF-A = 11).

(I) Quantification of CFU-GM number, CD45% and CD11b% in methylcellulose assays (700 Lin$^-$ HSPC were seeded). Vehicle (n = 8) or VEGF-A (4 μg/ml; n = 8) were added to standard culture medium.

Error bars, mean ± SEM. p values, two-tailed unpaired Student's t test. See also Figure S7.

AUTHOR CONTRIBUTIONS

Q.C., Y.L., and R.H.A. designed the study, interpreted results, and wrote the manuscript. Q.C. and Y.L. performed most experiments. H.-W.J. analyzed RNA-seq data and wrote part of the manuscript. M.S. performed FACS experiments. V.V.D. performed part of the FACS and immunostaining experiments. B.Z. provided critical mouse models.

DECLARATION OF INTERESTS

The authors declare no competing interests.

Received: April 23, 2019
Revised: August 2, 2019
Accepted: October 18, 2019
Published: November 21, 2019

REFERENCES

Aguirre, A., Blázquez-Prieto, J., Amado-Rodriguez, L., López-Alonso, I., Batalla-Solís, E., González-López, A., Sánchez-Pérez, M., Mayoral-Garcia, C., Gutiérrez-Fernández, A., and Albaiceta, G.M. (2017). Matrix metalloproteinase-14 triggers an anti-inflammatory proteolytic cascade in endotoxemia. J. Mol. Med. (Berl.) *95*, 487–497.

Asada, N., Kunisaki, Y., Pierce, H., Wang, Z., Fernandez, N.F., Birbrair, A., Ma'ayan, A., and Frenette, P.S. (2017). Differential cytokine contributions of perivascular haematopoietic stem cell niches. Nat. Cell Biol. *19*, 214–223.

Ballen, K.K., Gluckman, E., and Broxmeyer, H.E. (2013). Umbilical cord blood transplantation: the first 25 years and beyond. Blood *122*, 491–498.

Baryawno, N., Przybylski, D., Kowalczyk, M.S., Kfoury, Y., Severe, N., Gustafsson, K., Kokkaliaris, K.D., Mercier, F., Tabaka, M., Hofree, M., et al. (2019). A Cellular Taxonomy of the Bone Marrow Stroma in Homeostasis and Leukemia. Cell *177*, 1915–1932.

Bougaki, M., Searles, R.J., Kida, K., Yu, J., Buys, E.S., and Ichinose, F. (2010). Nos3 protects against systemic inflammation and myocardial dysfunction in murine polymicrobial sepsis. Shock *34*, 281–290.

Bowers, E., Slaughter, A., Frenette, P.S., Kuick, R., Pello, O.M., and Lucas, D. (2018). Granulocyte-derived TNFα promotes vascular and hematopoietic regeneration in the bone marrow. Nat. Med. *24*, 95–102.

Buch, T., Heppner, F.L., Tertilt, C., Heinen, T.J., Kremer, M., Wunderlich, F.T., Jung, S., and Waisman, A. (2005). A Cre-inducible diphtheria toxin receptor mediates cell lineage ablation after toxin administration. Nat. Methods *2*, 419–426.

Chen, Q., Zhang, H., Liu, Y., Adams, S., Eilken, H., Stehling, M., Corada, M., Dejana, E., Zhou, B., and Adams, R.H. (2016). Endothelial cells are progenitors of cardiac pericytes and vascular smooth muscle cells. Nat. Commun. *7*, 12422.

Comazzetto, S., Murphy, M.M., Berto, S., Jeffery, E., Zhao, Z., and Morrison, S.J. (2019). Restricted Hematopoietic Progenitors and Erythropoiesis Require SCF from Leptin Receptor+ Niche Cells in the Bone Marrow. Cell Stem Cell *24*, 477–486.

Copelan, E.A. (2006). Hematopoietic stem-cell transplantation. N. Engl. J. Med. *354*, 1813–1826.

Crane, G.M., Jeffery, E., and Morrison, S.J. (2017). Adult haematopoietic stem cell niches. Nat. Rev. Immunol. *17*, 573–590.

de Boer, J., Williams, A., Skavdis, G., Harker, N., Coles, M., Tolaini, M., Norton, T., Williams, K., Roderick, K., Potocnik, A.J., and Kioussis, D. (2003). Transgenic mice with hematopoietic and lymphoid specific expression of Cre. Eur. J. Immunol. *33*, 314–325.

del Toro, R., Prahst, C., Mathivet, T., Siegfried, G., Kaminker, J.S., Larrivee, B., Breant, C., Duarte, A., Takakura, N., Fukamizu, A., et al. (2010). Identification and functional analysis of endothelial tip cell-enriched genes. Blood *116*, 4025–4033.

Ding, L., Saunders, T.L., Enikolopov, G., and Morrison, S.J. (2012). Endothelial and perivascular cells maintain haematopoietic stem cells. Nature *481*, 457–462.

Doan, P.L., Himburg, H.A., Helms, K., Russell, J.L., Fixsen, E., Quarmyne, M., Harris, J.R., Deoliviera, D., Sullivan, J.M., Chao, N.J., et al. (2013a). Epidermal growth factor regulates hematopoietic regeneration after radiation injury. Nat. Med. *19*, 295–304.

Doan, P.L., Russell, J.L., Himburg, H.A., Helms, K., Harris, J.R., Lucas, J., Holshausen, K.C., Meadows, S.K., Daher, P., Jeffords, L.B., et al. (2013b). Tie2(+) bone marrow endothelial cells regulate hematopoietic stem cell regeneration following radiation injury. Stem Cells *31*, 327–337.

Dorris, S.L., and Peebles, R.S., Jr. (2012). PGI2 as a regulator of inflammatory diseases. Mediators Inflamm. *2012*, 926968.

Ehling, M., Adams, S., Benedito, R., and Adams, R.H. (2013). Notch controls retinal blood vessel maturation and quiescence. Development *140*, 3051–3061.

Ferrara, N., Carver-Moore, K., Chen, H., Dowd, M., Lu, L., O'Shea, K.S., Powell-Braxton, L., Hillan, K.J., and Moore, M.W. (1996). Heterozygous embryonic lethality induced by targeted inactivation of the VEGF gene. Nature *380*, 439–442.

Ferrara, J.L., Levine, J.E., Reddy, P., and Holler, E. (2009). Graft-versus-host disease. Lancet *373*, 1550–1561.

Gerber, H.P., Hillan, K.J., Ryan, A.M., Kowalski, J., Keller, G.A., Rangell, L., Wright, B.D., Radtke, F., Aguet, M., and Ferrara, N. (1999). VEGF is required for growth and survival in neonatal mice. Development *126*, 1149–1159.

Gerber, H.P., Malik, A.K., Solar, G.P., Sherman, D., Liang, X.H., Meng, G., Hong, K., Marsters, J.C., and Ferrara, N. (2002). VEGF regulates haematopoietic stem cell survival by an internal autocrine loop mechanism. Nature *417*, 954–958.

Greenbaum, A., Hsu, Y.M., Day, R.B., Schuettpelz, L.G., Christopher, M.J., Borgerding, J.N., Nagasawa, T., and Link, D.C. (2013). CXCL12 in early mesenchymal progenitors is required for haematopoietic stem-cell maintenance. Nature *495*, 227–230.

Guo, P., Poulos, M.G., Palikuqi, B., Badwe, C.R., Lis, R., Kunar, B., Ding, B.S., Rabbany, S.Y., Shido, K., Butler, J.M., and Rafii, S. (2017). Endothelial jagged-2 sustains hematopoietic stem and progenitor reconstitution after myelosuppression. J. Clin. Invest. *127*, 4242–4256.

Haigh, J.J., Morelli, P.I., Gerhardt, H., Haigh, K., Tsien, J., Damert, A., Miquerol, L., Muhlner, U., Klein, R., Ferrara, N., et al. (2003). Cortical and retinal defects caused by dosage-dependent reductions in VEGF-A paracrine signaling. Dev. Biol. *262*, 225–241.

Hassanshahi, M., Hassanshahi, A., Khabbazi, S., Su, Y.W., and Xian, C.J. (2017). Bone marrow sinusoidal endothelium: damage and potential regeneration following cancer radiotherapy or chemotherapy. Angiogenesis *20*, 427–442.

Helker, C.S., Schuermann, A., Pollmann, C., Chng, S.C., Kiefer, F., Reversade, B., and Herzog, W. (2015). The hormonal peptide Elabela guides angioblasts to the midline during vasculogenesis. eLife *4*. Published online May 27, 2015. https://doi.org/10.7554/eLife.06726.

Himburg, H.A., Muramoto, G.G., Daher, P., Meadows, S.K., Russell, J.L., Doan, P., Chi, J.T., Salter, A.B., Lento, W.E., Reya, T., et al. (2010). Pleiotrophin regulates the expansion and regeneration of hematopoietic stem cells. Nat. Med. *16*, 475–482.

Himburg, H.A., Sasine, J., Yan, X., Kan, J., Dressman, H., and Chute, J.P. (2016). A Molecular Profile of the Endothelial Cell Response to Ionizing Radiation. Radiat. Res. *186*, 141–152.

Himburg, H.A., Termini, C.M., Schlussel, L., Kan, J., Li, M., Zhao, L., Fang, T., Sasine, J.P., Chang, V.Y., and Chute, J.P. (2018). Distinct Bone Marrow Sources of Pleiotrophin Control Hematopoietic Stem Cell Maintenance and Regeneration. Cell Stem Cell *23*, 370–381.

Ho, L., van Dijk, M., Chye, S.T.J., Messerschmidt, D.M., Chng, S.C., Ong, S., Yi, L.K., Boussata, S., Goh, G.H., Afink, G.B., et al. (2017). ELABELA deficiency promotes preeclampsia and cardiovascular malformations in mice. Science *357*, 707–713.

Hoggatt, J., Kfoury, Y., and Scadden, D.T. (2016). Hematopoietic Stem Cell Niche in Health and Disease. Annu. Rev. Pathol. *11*, 555–581.

Hooper, A.T., Butler, J.M., Nolan, D.J., Kranz, A., Iida, K., Kobayashi, M., Kopp, H.G., Shido, K., Petit, I., Yanger, K., et al. (2009). Engraftment and reconstitution of hematopoiesis is dependent on VEGFR2-mediated regeneration of sinusoidal endothelial cells. Cell Stem Cell *4*, 263–274.

Itkin, T., Gur-Cohen, S., Spencer, J.A., Schajnovitz, A., Ramasamy, S.K., Kusumbe, A.P., Ledergor, G., Jung, Y., Milo, I., Poulos, M.G., et al. (2016). Distinct bone marrow blood vessels differentially regulate haematopoiesis. Nature *532*, 323–328.

Jeong, H.W., Hernández-Rodríguez, B., Kim, J., Kim, K.P., Enriquez-Gasca, R., Yoon, J., Adams, S., Schöler, H.R., Vaquerizas, J.M., and Adams, R.H. (2017). Transcriptional regulation of endothelial cell behavior during sprouting angiogenesis. Nat. Commun. *8*, 726.

Jin, Y., Wi, H.J., Choi, M.H., Hong, S.T., and Bae, Y.M. (2014). Regulation of anti-inflammatory cytokines IL-10 and TGF-β in mouse dendritic cells through treatment with Clonorchis sinensis crude antigen. Exp. Mol. Med. *46*, e74.

Kim, J. (2014). Apelin-APJ signaling: a potential therapeutic target for pulmonary arterial hypertension. Mol. Cells *37*, 196–201.

Knudsen, P.J., Dinarello, C.A., and Strom, T.B. (1986). Prostaglandins post-transcriptionally inhibit monocyte expression of interleukin 1 activity by increasing intracellular cyclic adenosine monophosphate. J. Immunol. *137*, 3189–3194.

Kondo, M., Wagers, A.J., Manz, M.G., Prohaska, S.S., Scherer, D.C., Beilhack, G.F., Shizuru, J.A., and Weissman, I.L. (2003). Biology of hematopoietic stem cells and progenitors: implications for clinical application. Annu. Rev. Immunol. *21*, 759–806.

Kuba, K., Sato, T., Imai, Y., and Yamaguchi, T. (2019). Apelin and Elabela/Toddler; double ligands for APJ/Apelin receptor in heart development, physiology, and pathology. Peptides *111*, 62–70.

Kusumbe, A.P., Ramasamy, S.K., and Adams, R.H. (2014). Coupling of angiogenesis and osteogenesis by a specific vessel subtype in bone. Nature *507*, 323–328.

Kusumbe, A.P., Ramasamy, S.K., Itkin, T., Mäe, M.A., Langen, U.H., Betsholtz, C., Lapidot, T., and Adams, R.H. (2016). Age-dependent modulation of vascular niches for haematopoietic stem cells. Nature *532*, 380–384.

Langen, U.H., Pitulescu, M.E., Kim, J.M., Enriquez-Gasca, R., Sivaraj, K.K., Kusumbe, A.P., Singh, A., Di Russo, J., Bixel, M.G., Zhou, B., et al. (2017). Cell-matrix signals specify bone endothelial cells during developmental osteogenesis. Nat. Cell Biol. *19*, 189–201.

Li, X.M., Hu, Z., Jorgenson, M.L., Wingard, J.R., and Slayton, W.B. (2008). Bone marrow sinusoidal endothelial cells undergo nonapoptotic cell death and are replaced by proliferating sinusoidal cells in situ to maintain the vascular niche following lethal irradiation. Exp. Hematol. *36*, 1143–1156.

Liu, Q., Hu, T., He, L., Huang, X., Tian, X., Zhang, H., He, L., Pu, W., Zhang, L., Sun, H., et al. (2015). Genetic targeting of sprouting angiogenesis using Apln-CreER. Nat. Commun. *6*, 6020.

Manicone, A.M., and McGuire, J.K. (2008). Matrix metalloproteinases as modulators of inflammation. Semin. Cell Dev. Biol. *19*, 34–41.

Mann, M., Mehta, A., de Boer, C.G., Kowalczyk, M.S., Lee, K., Haldeman, P., Rogel, N., Knecht, A.R., Farouq, D., Regev, A., et al. (2018). Heterogeneous Responses of Hematopoietic Stem Cells to Inflammatory Stimuli Are Altered with Age. Cell Rep *25*, 2992–3005.

Maxwell, P.J., Longley, D.B., Latif, T., Boyer, J., Allen, W., Lynch, M., McDermott, U., Harkin, D.P., Allegra, C.J., and Johnston, P.G. (2003). Identification of 5-fluorouracil-inducible target genes using cDNA microarray profiling. Cancer Res. *63*, 4602–4606.

Mendelson, A., and Frenette, P.S. (2014). Hematopoietic stem cell niche maintenance during homeostasis and regeneration. Nat. Med. *20*, 833–846.

Méndez-Ferrer, S., Michurina, T.V., Ferraro, F., Mazloom, A.R., Macarthur, B.D., Lira, S.A., Scadden, D.T., Ma'ayan, A., Enikolopov, G.N., and Frenette, P.S. (2010). Mesenchymal and haematopoietic stem cells form a unique bone marrow niche. Nature *466*, 829–834.

Morgan, R.A., Gray, D., Lomova, A., and Kohn, D.B. (2017). Hematopoietic Stem Cell Gene Therapy: Progress and Lessons Learned. Cell Stem Cell *21*, 574–590.

Muzumdar, M.D., Tasic, B., Miyamichi, K., Li, L., and Luo, L. (2007). A global double-fluorescent Cre reporter mouse. Genesis *45*, 593–605.

Noach, E.J., Ausema, A., van Os, R., Akkerman, I., Koopal, S., Weersing, E., Dontje, B., Vellenga, E., and de Haan, G. (2003). Chemotherapy prior to autologous bone marrow transplantation impairs long-term engraftment in mice. Exp. Hematol. *31*, 528–534.

Pietras, E.M. (2017). Inflammation: a key regulator of hematopoietic stem cell fate in health and disease. Blood *130*, 1693–1698.

Pitulescu, M.E., Schmidt, I., Giaimo, B.D., Antoine, T., Berkenfeld, F., Ferrante, F., Park, H., Ehling, M., Biljes, D., Rocha, S.F., et al. (2017). Dll4 and Notch signalling couples sprouting angiogenesis and artery formation. Nat. Cell Biol. *19*, 915–927.

Rafii, S., and Lyden, D. (2003). Therapeutic stem and progenitor cell transplantation for organ vascularization and regeneration. Nat. Med. *9*, 702–712.

Rafii, S., Butler, J.M., and Ding, B.S. (2016). Angiocrine functions of organ-specific endothelial cells. Nature *529*, 316–325.

Ramasamy, S.K., Kusumbe, A.P., Itkin, T., Gur-Cohen, S., Lapidot, T., and Adams, R.H. (2016). Regulation of Hematopoiesis and Osteogenesis by Blood Vessel-Derived Signals. Annu. Rev. Cell Dev. Biol. *32*, 649–675.

Ratajczak, M.Z., and Suszynska, M. (2016). Emerging Strategies to Enhance Homing and Engraftment of Hematopoietic Stem Cells. Stem Cell Rev Rep *12*, 121–128.

Rocha, S.F., Schiller, M., Jing, D., Li, H., Butz, S., Vestweber, D., Biljes, D., Drexler, H.C., Nieminen-Kelhä, M., Vajkoczy, P., et al. (2014). Esm1 modulates endothelial tip cell behavior and vascular permeability by enhancing VEGF bioavailability. Circ. Res. *115*, 581–590.

Severe, N., Karabacak, N.M., Gustafsson, K., Baryawno, N., Courties, G., Kfoury, Y., Kokkaliaris, K.D., Rhee, C., Lee, D., Scadden, E.W., et al. (2019). Stress-Induced Changes in Bone Marrow Stromal Cell Populations Revealed through Single-Cell Protein Expression Mapping. Cell Stem Cell *25*, 570–583.

Slayton, W.B., Li, X.M., Butler, J., Guthrie, S.M., Jorgensen, M.L., Wingard, J.R., and Scott, E.W. (2007). The role of the donor in the repair of the marrow vascular niche following hematopoietic stem cell transplant. Stem Cells *25*, 2945–2955.

Sugiyama, T., Kohara, H., Noda, M., and Nagasawa, T. (2006). Maintenance of the hematopoietic stem cell pool by CXCL12-CXCR4 chemokine signaling in bone marrow stromal cell niches. Immunity *25*, 977–988.

Taniguchi Ishikawa, E., Gonzalez-Nieto, D., Ghiaur, G., Dunn, S.K., Ficker, A.M., Murali, B., Madhu, M., Gutstein, D.E., Fishman, G.I., Barrio, L.C., and Cancelas, J.A. (2012). Connexin-43 prevents hematopoietic stem cell senescence through transfer of reactive oxygen species to bone marrow stromal cells. Proc. Natl. Acad. Sci. USA *109*, 9071–9076.

Thomas, E., Storb, R., Clift, R.A., Fefer, A., Johnson, F.L., Neiman, P.E., Lerner, K.G., Glucksberg, H., and Buckner, C.D. (1975). Bone-marrow transplantation (first of two parts). N. Engl. J. Med. *292*, 832–843.

Tian, X., Hu, T., Zhang, H., He, L., Huang, X., Liu, Q., Yu, W., He, L., Yang, Z., Zhang, Z., et al. (2013). Subepicardial endothelial cells invade the embryonic ventricle wall to form coronary arteries. Cell Res. *23*, 1075–1090.

Tikhonova, A.N., Dolgalev, I., Hu, H., Sivaraj, K.K., Hoxha, E., Cuesta-Dominguez, A., Pinho, S., Akhmetzyanova, I., Gao, J., Witkowski, M., et al. (2019). The bone marrow microenvironment at single-cell resolution. Nature *569*, 222–228.

Wang, Y., Nakayama, M., Pitulescu, M.E., Schmidt, T.S., Bochenek, M.L., Sakakibara, A., Adams, S., Davy, A., Deutsch, U., Lüthi, U., et al. (2010). Ephrin-B2 controls VEGF-induced angiogenesis and lymphangiogenesis. Nature *465*, 483–486.

Wu, S., Wu, Y., and Capecchi, M.R. (2006). Motoneurons and oligodendrocytes are sequentially generated from neural stem cells but do not appear to share common lineage-restricted progenitors in vivo. Development *133*, 581–590.

Xu, C., Gao, X., Wei, Q., Nakahara, F., Zimmerman, S.E., Mar, J., and Frenette, P.S. (2018). Stem cell factor is selectively secreted by arterial endothelial cells in bone marrow. Nat. Commun. *9*, 2449.

Yahyapour, R., Salajegheh, A., Safari, A., Amini, P., Rezaeyan, A., Amraee, A., and Najafi, M. (2018). Radiation-induced Non-targeted Effect and Carcinogenesis; Implications in Clinical Radiotherapy. J. Biomed. Phys. Eng. *8*, 435–446.

Zhao, M., Perry, J.M., Marshall, H., Venkatraman, A., Qian, P., He, X.C., Ahamed, J., and Li, L. (2014). Megakaryocytes maintain homeostatic quiescence and promote post-injury regeneration of hematopoietic stem cells. Nat. Med. *20*, 1321–1326.

Zhou, B.O., Ding, L., and Morrison, S.J. (2015). Hematopoietic stem and progenitor cells regulate the regeneration of their niche by secreting Angiopoietin-1. eLife *4*, e05521.

STAR★METHODS

KEY RESOURCES TABLE

REAGENT or RESOURCE	SOURCE	IDENTIFIER(RRID)
Antibodies		
Endomucin	Santa Cruz	RRID:AB_2100037
GFP-Alexa488	Invitrogen	RRID:AB_221477
CD31	R&D	RRID:AB_2161028
Collagen IV	AbD Serotec	RRID:AB_2082660
ERG	Abcam	RRID:AB_10864794
PDGFR-beta	eBioscience	RRID:AB_467493
VEGFR2	R&D	RRID:AB_355500
VEGFR3	R&D	RRID:AB_355563
BCAM	R&D	RRID:AB_2811217
Caveolin-1	Cell signaling	RRID:AB_2072166
Lineage-biotin cocktail	Miltenyi Biotec	RRID:AB_1103214
CD150-Alexa647	Biolegend	RRID:AB_2239178
CD48-biotin	eBioscience	RRID:AB_466470
Caspase3	Cell Signaling	RRID:AB_2341188
B220-biotin	BD pharmingen	RRID:AB_10053179
RFP (Tomato)	MBL	RRID:AB_591279
Ki67	Abcam	RRID:AB_443209
VE-cadherin	R&D	RRID:AB_2077789
Sca-1	Biolegend	RRID:AB_756190
αSMA	eBioscience	RRID:AB_2574362
Linegae-biotin cocktail	Miltenyi Biotec	RRID:AB_1103214
Sca1-FITC	eBioscience	RRID:AB_465334
cKit-APC	BD pharmingen	RRID:AB_398536
Ter119-APC	eBioscience	RRID:AB_469474
CD45-FITC	eBioscience	RRID:AB_465049
CD45R(B220)-APC	Invitrogen	RRID:AB_10392558
Ly-6G-APC	eBioscience	RRID:AB_469475
CD11b-APC	Biolegend	RRID:AB_312795
CD3-APC	eBioscience	RRID:AB_469313
CD4-APC	eBioscience	RRID:AB_469323
CD8-APC	eBioscience	RRID:AB_469335
CD150-PE	Biolegend	RRID:AB_313683
CD48-APC-Cy7	BD pharmingen	RRID:AB_10644381
CD34-eFluor450	eBioscience	RRID:AB_2043837
CD127-PE	eBioscience	RRID:AB_465845
CD16/CD32 PE-Cy7	eBioscience	RRID:AB_469598
Ter-119 Pacific Blue	Biolegend	RRID:AB_2251160
CD45- Pacific Blue	Biolegend	RRID:AB_493535
CD51-PE	eBioscience	RRID:AB_465704
CD140a-APC	eBioscience	RRID:AB_529482
CD140b-APC	eBioscience	RRID:AB_1548743
Lepr-biotin	R&D	RRID:AB_2296953
CD31-Alexa488	R&D	RRID:AB_10972784
CD31-APC	R&D	RRID:AB_10971931

(*Continued on next page*)

Continued

REAGENT or RESOURCE	SOURCE	IDENTIFIER(RRID)
Cdh5-APC	eBioscience	RRID:AB_10598508
CD31-Pe/Cy7	Biolegend	RRID:AB_2572182
Endomucin	Santa Cruz	RRID:AB_2100037
CD45.1-FITC	invitrogen	RRID:AB_2539698
CD45.2 Pacific Blue	Biolegend	RRID:AB_492872
CD45 PE-Cy7	eBioscience	RRID:AB_2734986
Annexin V-APC	BD pharmingen	550474
Anti-biotin Microbeads	Miltenyi Biotec	RRID:AB_2811216
Biological Samples		
Mouse blood	This paper	N/A
Mouse bone marrow cells	This paper	N/A
Mouse spleen, retina, heart, skin, small intestine	This paper	N/A
Chemicals, Peptides, and Recombinant Proteins		
Human recombinant VEGF-A	Reliatech	300-076
Dextran Texas Red	ThermoFisher Scientific	D1830
MethoCult^{Tm} medium	Stem cell technologies	GF M3434
EdU	Thermofisher scientific	A10044,
Tamoxifen	Sigma	T5648
4OH-tamoxifen	Sigma	H7904
Peanut oil	Sigma	P2144
Vybrant DyeCycle Violet stain	Invitrogen	V35003
Critical Commercial Assays		
Legendplex mouse inflammation panel	Biolegend	740446
Mouse VEGF-A ELISA Kit	Cloud-Clone Corp	SEA143Mu
SMART-Seq v4 Ultra Low Input RNA kit for Sequencing	Takara	634894
Nextera XT DNA Library Preparation Kit	Illumina	15031942
Click-iT EdU Alexa-647 imaging Kit	Invitrogen	C10340
RNeasy plus Micro Kit	QIAGEN	74034
iScript^{TM} cDNA Synthesis Kit	BioRad	170-8891
Deposited Data		
RNA sequencing	This paper	GSE115422
Experimental Models: Cell Lines		
bEnd.3	ATCC	ATCC CRL-2299
Experimental Models: Organisms/Strains		
Cdh5 membrane-Tdtomato H2B-EGFP(Cdh5-mTnG)	Our lab	PMID: 28959057
Rosa26-mT/mG	The Jackson Laboratory	RRID:IMSR_JAX:007576
Cdh5(PAC)-CreERT2	Our lab	RRID:MGI:3848984
Apln-CreERT2	Bin Z lab	PMID: 23797856
Bmx-CreERT2	Our lab	PMID: 23785053
Vav1-Cre	The Jackson Laboratory	RRID:IMSR_JAX:008610
VEGFa^{tm2Gne}	Ferrara N lab	PMID: 10021335
Kdr^{tm1Wag}	Nagy A lab	PMID: 14550787
Rosa26-DTR	The Jackson Laboratory	RRID:IMSR_JAX:007900
Rosa26-DTA$^{tm1(DTA)Mrc}$	The Jackson Laboratory	RRID:IMSR_JAX:010527)
Kitl	The Jackson Laboratory	RRID:IMSR_JAX:017861
Esm1-CreERT2	Our lab	PMID: 25057127

(*Continued on next page*)

Continued

REAGENT or RESOURCE	SOURCE	IDENTIFIER(RRID)
Software and Algorithms		
Fiji	NIH	ImageJ 1.51 s
Volocity	PerkinElmer	6.3
Photochop	Adobe	CS6
Illustrator	Adobe	CS6
Graphpad Prism	GraphPad	7
Microsoft Excel	Microsoft	15.40
FACS Diva	BD	8.0.1
FACSuite	BD	1.0.5.3841
Legendplex	Biolegend	8.0
FlowJo	BD	10.4.2
TopHat	John Hopkins Univ.	version 2.1.1
HTSeq-count	PMID: 25260700	version 0.6.1
DESeq2	Bioconductor	version 3.9

LEAD CONTACT AND MATERIALS AVAILABILITY

Further information and requests for resources and reagents should be directed to and will be fulfilled by the Lead Contact, Ralf H. Adams (ralf.adams@mpi-muenster.mpg.de). This study did not generate new unique reagents.

EXPERIMENTAL MODEL AND SUBJECT DETAILS

8-15 week-old mice were used as young adults and C57BL/6 males were used as wild-type mice for all analysis unless stated otherwise. Genetically modified mouse models used in this study are summarized in Table S1. Littermates with appropriate genotypes were used as controls of genetically modified mutants whenever possible (see further details below).

Cdh5(PAC)-mtdTomato-nGFP (*Cdh5-mTnG*) reporter mice were previously described and used for labeling of EC nuclei and FACS-sorting (Jeong et al., 2017).

Vav1-Cre (de Boer et al., 2003) transgenic mice were interbred with *Rosa26-DTR (Buch et al., 2005)* animals to generate *Vav1-Cre*$^{+/T}$ *Rosa26-DTR*$^{+/lox}$ (*DTR*$^{i\Delta HC}$) mice. *Vav1-Cre*$^{+/+}$ *Rosa26-DTR*$^{+/lox}$ littermates were used as controls. 25 μg/kg diphtheria toxin (Sigma, D0564) was administrated to *DTR* $^{i\Delta HC}$ and control mice for 2 consecutive days and animals were analyzed 4 days after first injection. *DTR* $^{i\Delta HC}$ mutants were interbred with *Cdh5-mTnG* animals to generate *Vav1-Cre*$^{+/T}$ *Rosa26-DTR*$^{+/lox}$ *Cdh5-mTnG*$^{+/T}$ triple transgenic mice for the visualization of EC nuclei and flow cytometry analysis. *Vav1-Cre* transgenic mice were interbred with conditional (floxed) *Vegfa* mutants (Gerber et al., 1999) mice to generate *Vav1-Cre*$^{+/T}$ *Vegfa*$^{+/lox}$ (*Vegfa*$^{\Delta HC}$) animals and *Vav1-Cre*$^{+/+}$ *Vegfa*$^{+/lox}$ controls. *Vav1-Cre* transgenic mice were also interbred with conditional (floxed) *Kdr (Vegfr2)* (Haigh et al., 2003) mutants to generate *Vav1-Cre*$^{+/T}$ *Kdr*$^{lox/lox}$ (*Vegfr2*$^{\Delta HC}$) mice and *Vav1-Cre*$^{+/+}$ *Kdr*$^{lox/lox}$ controls.

In the *Rosa26-mTmG* reporter (Muzumdar et al., 2007) background, Cre activity leads to an irreversible switch from constitutive membrane-anchored tdTomato protein expression to membrane-anchored GFP. *Cdh5(PAC)-CreERT2* (Wang et al., 2010) transgenic mice were interbred with *Rosa26-mTmG* reporter animals to generate *Cdh5-CreERT2 Rosa26-mTmG* mice enabling genetic labeling of all ECs. For the morphological analysis of ECs at single cell level, 10 μg tamoxifen (Sigma, T5648) were injected to *Cdh5-CreERT2 Rosa26-mTmG mice* 6 days after irradiation or 5-FU treatment. *Bmx-CreERT2* (Ehling et al., 2013) transgenic mice were interbred with the *Rosa26-mTmG* strain to generate *Bmx-CreERT2 Rosa26-mTmG* for genetic labeling of arterial ECs. 500 μg tamoxifen were administered on 2 consecutive days to *Bmx-CreERT2 Rosa26-mTmG* mice for analysis in irradiation experiments with or without transplantation.

Apln-CreERT2 (T/y) hemizygous males were used for all experiments with this strain to avoid mosaic Cre recombinase expression due to X-inactivation in (T/x) heterozygous females (Tian et al., 2013). *Apln-CreERT2* transgenic animals were bred into the *Rosa26-mTmG* background to generate *Apln-CreERT2 Rosa26-mTmG* (*Apln-mTmG*) mice for genetic labeling, lineage tracing and flow cytometry analysis of Apln+ ECs in bone. 1mg tamoxifen was injected intraperitoneally to *Apln-mTmG* mice on three consecutive days for the labeling and flow cytometric analysis of Apln+ ECs. 1mg 4-hydroxytamoxifen (4-OHT; Sigma, H7904) was injected intraperitoneally at 1 day before irradiation for lineage tracing of Apln+ ECs and their descendants after transplantation. *Apln-CreERT2* transgenic mice were interbred with *Rosa26-DTA* (Wu et al., 2006) animals to generate *Apln-CreERT2*$^{T/y}$ *Rosa26-DTA*$^{lox/lox}$ (*DTA*$^{i\Delta Apln}$) males and *Apln-CreERT2*$^{+/y}$ *Rosa26-DTA*$^{lox/lox}$ controls. Two injections of 1mg tamoxifen were used to induce CreERT2 activity and the ablation of Apln+ ECs (Figure S4M). *Apln-CreERT2* transgenic mice were interbred with *Kdr* conditional (floxed) animals to generate *Apln-CreERT2*$^{T/y}$ *Kdr*$^{lox/lox}$ (*Vegfr2*$^{i\Delta Apln}$) mutants and *Apln-CreERT2*$^{+/y}$ *Kdr*$^{lox/lox}$ controls. 2 mg tamoxifen were injected

on 5 consecutive days to *Vegfr2*$^{i\Delta Apln}$ and control mice for transplantation experiments. *Apln-CreERT2* transgenic mice were interbred with *Kitl*$^{tm2.1Sjm}$ (encoding SCF) conditional (floxed) animals to generate *Apln-CreERT2*$^{T/y}$ *Kitl*$^{lox/lox}$ (*Kitl*$^{i\Delta Apln}$) mutants and *Apln-CreERT2*$^{+/y}$ *Kitl*$^{lox/lox}$ controls. 2mg tamoxifen were injected on 5 consecutive days to *Kitl*$^{i\Delta Apln}$ and control mice for analysis.

Cdh5(PAC)-CreERT2 transgenic mice were interbred with *Kdr* conditional (floxed) animals to generate *Cdh5(PAC)-CreERT2*$^{+/T}$ *Kdr*$^{lox/lox}$ (*Vegfr2*$^{i\Delta EC}$) mutants and *Cdh5(PAC)-CreERT2*$^{+/+}$ *Kdr*$^{lox/lox}$ controls. 1mg tamoxifen was injected on 5 consecutive days to *Vegfr2* $^{i\Delta EC}$ and control mice for transplantation experiments. *Esm1-CreERT2* transgenic mice were interbred with *Rosa26-mTmG* and *Rosa26-DTA* animals to generate *Esm1-CreERT2*$^{+/T}$ *Rosa26-mTmG* and *Esm1-CreERT2*$^{+/T}$ *Rosa26-DTA* (*DTA*$^{i\Delta Esm1}$) mice. *Esm1-Cre* mice were treated with exactly the same tamoxifen injection protocol as *Apln-Cre* animals (Figures S6H and S6L).

All animals were routinely genotyped using respective PCR protocols. Protocols and primer sequences can be provided upon request. All the animals were housed in the animal facility at the Max Planck Institute for Molecular Biomedicine or the Institute for Nutritional Sciences and Shanghai Institute of Biochemistry and Cell Biology, Shanghai Institute for Biological Sciences, Chinese Academy of Sciences. All experiments were performed according to the institutional guidelines and laws, following the protocols approved by local and national animal ethics committees.

METHOD DETAILS

Cryosectioning, immunohistochemistry and permeability assays

Adult bones were dissected and immediately placed in ice-cold 4% paraformaldehyde (PFA-PBS) solution and fixed under gentle agitation overnight. Bone samples were placed in 0.5M EDTA (Ph 8.0) for at least 2 days, dehydrated in 20% sucrose-1% polyvinylpyrrolidone PBS solution for at least 2 days, and embedded in PBS containing 15% sucrose, 8% gelatin and 1% polyvinylpyrrolidone for storage at −80°C and cryosectioning on a Leica CM3050 cryostat using low profile blades. For immunostaining, bone sections were rehydrated in PBS, permeabilized for 15 min in 0.5% Triton X-100 PBS solution and blocked for 30 min in PBS containing 1% BSA, 2% donkey serum, 0.3% Trion X100 PBS (blocking buffer) at room temperature. Sections were probed with primary antibodies diluted in blocking buffer at 4°C overnight. After incubation, sections were washed three times with PBS and incubated with appropriate Alexa Fluor-conjugated secondary antibodies (1:100 to 1:400, Invitrogen) diluted in blocking buffer at room temperature for 2 hours. Nuclei were stained with DAPI during secondary antibody incubation. After that, sections were washed three times with PBS, mounted with Fluoromount-G (0100-01, Southern Biotech) and kept in 4°C for imaging.

For the analysis of vascular permeability in bone, 1mg Dextran Texas Red (ThermoFisher Scientific, D1830, 70000MW) was injected into the tail vein. Mice were sacrificed 15 minutes after injection. Femurs were dissected and directly placed in ice-cold 4% PFA for overnight fixation. Further processing of femur samples was exactly the same as for immunostainings. Texas Red signal was excited with a 594nm laser during confocal microscope without signal enhancement.

Flow cytometry

Bones were dissected and crushed by pestle for more than 3 times before cells were collected in 2% FCS-PBS solution. The tissue was immersed in 6ml dissociation solution (2% FCS-PBS solution with approximate 145U/ml type 4 GIBCO collagenase) and incubated at 37°C for 30 minutes. Samples were filtered using 70 μm Nylon cell strainer to get single cell suspensions. Reporter mice expressing fluorescent proteins were directly used for flow cytometry. Primary antibodies were diluted in 2% FCS-PBS solution and incubated with cells on ice for 40 minutes. Cells were washed 3 times by 2% FCS-PBS solution and incubated with secondary antibodies for 40 minutes. Cells were washed 3 further times again and used for flow cytometry. Cells were resuspended in PBS/2% FCS supplemented with 1 μg/ml DAPI to allow exclusion of nonviable cells when required. Cell sorting was performed on a FACSAriaIIu cell sorter (BD Biosciences, San Jose, CA) using an 85 μm nozzle. Cell analysis was performed using BD FACS Verse.

Irradiation, transplantation, lineage separation and VEGF-A treatment

Mice were exposed to a lethal dose of Gamma irradiation (137Cs, GammaCell 40, Best Theratronics) of 9 Gy and typically analyzed 7 days after irradiation (shown as "9 Gy" in the results), unless another experimental regime is mentioned in the legend. Bone marrow cells (or Lin-/LSK cells) were transplanted 4 to 6 hours after irradiation. For competitive long-term repopulating assays, CD45.1 host mice were lethally irradiated (12 Gy) and transplanted with 5×10^5 donor-derived (CD45.2 background) BM cells together with 5×10^5 host-derived (CD45.1 background) bone marrow cells. Host mice were sacrificed about 16 weeks after transplantation to determine chimerism in bone marrow and peripheral blood using FACS analysis.

For separation of lineage-positive cells, bone marrow cells were collected and filtered as described for flow cytometry analysis. Biotinylated-lineage cocktail antibodies (Miltenyi Biotec, 130-092-613) were mixed with cells at 4°C for 20 minutes. Antibody-conjugated BM cells were washed 2 times and then incubated with anti-biotin antibody-conjugated magnetic microbeads (Miltenyi Biotec, 130-105-637) at 4°C for 30 minutes. The cells were washed 2 times and separated with LS column (MiltenyiBiotec, 130-042-401). Lineage negative or positive cells were counted and transplanted as outlined in the relevant results.

In VEGF-A treatment experiments, 10^4 lineage-negative cells were transplanted together with 2 μg VEGF-A (Reliatech, 300-076) 4 to 6 hours after lethal irradiation. In the following days, 2 μg VEGF-A or vehicle (PBS) were intravenously injected into recipients as indicated in Figure 7C. 3 weeks after irradiation, vehicle and VEGF-A treated mice were sacrificed for analysis or for secondary transplantation (long-term repopulating assays). Before intravenous injection, VEGF-A activity was validated in culture ECs.

Blood count, blood plasma cytokine analysis and bone marrow cell number counting

Peripheral blood was extracted from the submandicular vein, collected in EDTA-K tube and analyzed with a Scil Vet ABC plus according to the manufacturer's instructions. To analyze peripheral blood cells using FACS, whole blood was centrifuged at 1000 g for 10 minutes and blood plasma was separated. Blood cells layers were resuspended for FACS analysis. The remaining blood plasma was used to calculate cytokine levels by using the Biolegend Legendplex mouse inflammation panel (13-plex; Biolegend, 740446). The experimental process and quantification analysis were performed following the manufacturer's protocol. Data analysis was performed using software provided by Biolegend. Manual gating was used to define beads A and B, while an automatic gating strategy was used to gate individual cytokine in APC-PE plot. Cytokine levels lower than detection level were excluded from analysis.

For counting of BM nucleated cells, BM cells were processed to generate single cell suspensions, as described for flow cytometry analysis. Red blood cells were removed using RBC lysis buffer (ebioscience, 00-4300-54). Total cell numbers were determined using cell counting plates or a Luna 2 automated cell counter (Logos Biosystems). The number of different cell types in BM was calculated based on BMNC counting and flow cytometry analysis with appropriate markers.

ELISA

To collect bone marrow supernatant for ELISA analysis, 1 femur was dissected, flushed into 1ml PBS solution and immediately kept on ice. Solutions were centrifuged at 300 g for 5 minutes. Supernatant was stored at −80°C. To collect BM cellular protein for ELISA analysis, Lin- and Lin+ cells were separated. After counting the number of cells, Lin- or Lin+ cells were centrifuged and immersed in NP40 solution with proteinase inhibitor cocktail. The cell-NP40 solution was rotated at 4°C for 30 minutes and then centrifuged at 15000 g for 30 minutes. The remaining supernatant was collected and stored at −80°C. ELISA for VEGF-A was performed with a kit following the manufacturer's instructions (Cloud-Clone Corp, SEA143Mu).

In vitro methycellulose and bEnd.3 assays

Approximate 700 Lin- cells from wild-type mice were magnetically separated and cultured in MethoCult^{Tm} medium (GF M3434, Stem cell technologies) in a 35mm dish. 4μg/ml VEGF-A or vehicle (PBS) were added to the MethoCult^{Tm} medium for *in vitro* culture. Lin- HSPCs from the same batch were equally distributed, then exposed to vehicle (PBS) or VEGF-A for half an hour before seeding. Cells and medium were incubated in 37°C 5%CO_2 cell incubator. 7 days after incubation, CFU number was counted. After counting, cells were washed 4 times with 2% FCS-PBS solution and filtered with 70 μm Nylon cell strainer to get single cell solution for FACS analysis. The FACS staining protocol was the same as for BM cells (see above).

bEnd.3 endothelial cells were cultured in base medium (including DMEM, Glutamine and P/S) plus 5% FCS in 37°C incubator with 5% CO_2. Cells were passaged into 6 well-plates and, at 70%–80% confluency, the culture medium was changed to base medium plus 1μg/ml VEGF-A or base medium plus PBS vehicle without any serum. The cells were collected into RLT lysis buffer for RNA extraction at 24 hours after a final culture medium change.

EdU incorporation

EdU (A10044, Thermofisher scientific) was dissolved in PBS. 40mg/kg EdU-PBS was injected to *Cdh5-mTnG* mice at 7 consecutive days after irradiation. Bone samples were processed as described above. Click-iT EdU Alexa-647 imaging Kit (C10340, Invitrogen) was used to visualize EdU signals. Single optical slices instead of z stacked images were used for data analysis. Co-localization of GFP and EdU signal were analyzed and recorded in Volocity (PerkinElmer).

RNA extraction and quantitative PCR

RNA was extracted using RNeasy plus Micro Kit (74034, QIAGEN) and cDNA was generated with iScript^{TM} cDNA Synthesis Kit (#170-8891, BioRad). Quantitative PCR with reverse transcription was performed with a Bio-rad CFX96 real-time PCR system using FAM-conjugated Taqman probes for *Vegfa* (Mm00437306_m1) and *Apln* (Mm00443562_m1). Gene expression levels were normalized to the endogenous VIC-conjugated *Actb* probe (4352341E) as control.

RNA sequencing and data analysis

Total RNAs were extracted using RNeasy Plus Micro kit (QIAGEN) according to the manufacturer's instructions. Quality and quantity of RNA samples were analyzed with a Bioanalyzer and RNA 6000 pico kit (Agilent). Double strand cDNA was synthesized using SMART-Seq v4 Ultra Low Input RNA kit for Sequencing (Takara) and sequencing libraries were constructed with Nextera XT DNA Library Preparation Kit (Illumina) according to the manufacturer's instructions. TruSeq Stranded Total RNA kit (Illumina) was used for the library preparation of total BMC and Lin- samples. The resulting sequencing library was sequenced with 2 × 75 bp paired-end reads on MiSeq or NextSeq 500 sequencer (Illumina). Sequenced reads were aligned to the mouse (mm10) reference genome with TopHat (version 2.1.1), and the aligned reads were used for the transcript quantification by using HTSeq-count (version 0.6.1). DESeq2 was used to identify differentially expressed genes across the samples.

Raw data for Lepr+ and NG2+ cells were derived from previous work (Asada et al., 2017) (GEO accession number: GSE89811).

Confocal imaging and image processing

Stained bone sections were imaged with laser scanning confocal microscopes (Leica SP5 or SP8, Zeiss LSM780) after immunohistochemistry. Quantitative analysis of mutant phenotypes was done with the same microscope and identical imaging acquisition

setting for mutant and control samples. Overview images of bone were automatically generated using the tile-scan function of SP5 and LSM780 associated software and the resulting pictures combine multiple individual maximum intensity images. Maximum projections were generated by Volocity or Fiji. Volocity (PerkinElmer), Fiji (open source; http://fiji.sc/), Photoshop and Illustrator (Adobe) softwares were used for image processing in compliance with *Cell Stem Cell*'s guide for digital images. In general, original images were loaded into Volocity and brightness-contrast modifications were applied to the whole image. Images exported from Volocity were rotated and cropped in Fiji. Quantification of cell number, length, and area was performed in Volocity and Fiji. Shape factor is a numerical indication of how similar a 2D shape is to a perfect circle. A shape factor of 1 indicates a perfect sphere.

QUANTIFICATION AND STATISTICAL ANALYSIS

No statistical methods were used to predetermine sample size. Mice that died before the completion of experimental protocols were excluded from analysis, which was a pre-established criterion before the experiment. No randomization and blinding were used. Samples were tested using two-tailed Student's t test. *P value* less than 0.05 was considered to be statistically significant. Statistical data were drawn from normally distributed group. Before the Student's *t*-Test, samples from different groups were tested using *F*-test to identify the variances between groups. *F* value less than 0.05 indicated samples have significantly different variances. All results are represented as mean ± s.e.m. Number of animals or cells represents biological replicates.

DATA AND CODE AVAILABILITY

RNA-seq raw data supporting this work have been deposited in GEO, under accession number GSE115422. All original data are available upon reasonable request to Lead Contact.

Cell Stem Cell, Volume *25*

Supplemental Information

Apelin^{+} Endothelial Niche Cells Control Hematopoiesis and Mediate Vascular Regeneration after Myeloablative Injury

Qi Chen, Yang Liu, Hyun-Woo Jeong, Martin Stehling, Van Vuong Dinh, Bin Zhou, and Ralf H. Adams

Supplemental Information for

Apelin^{+} Endothelial Niche Cells Control Hematopoiesis and Mediate Vascular Regeneration after Myeloablative Injury

Qi Chen, Yang Liu, Hyun-Woo Jeong, Martin Stehling, Van Vuong Dinh, Bin Zhou, Ralf H. Adams

This PDF file includes:

Supplemental Figures and Legends

Supplemental Tables

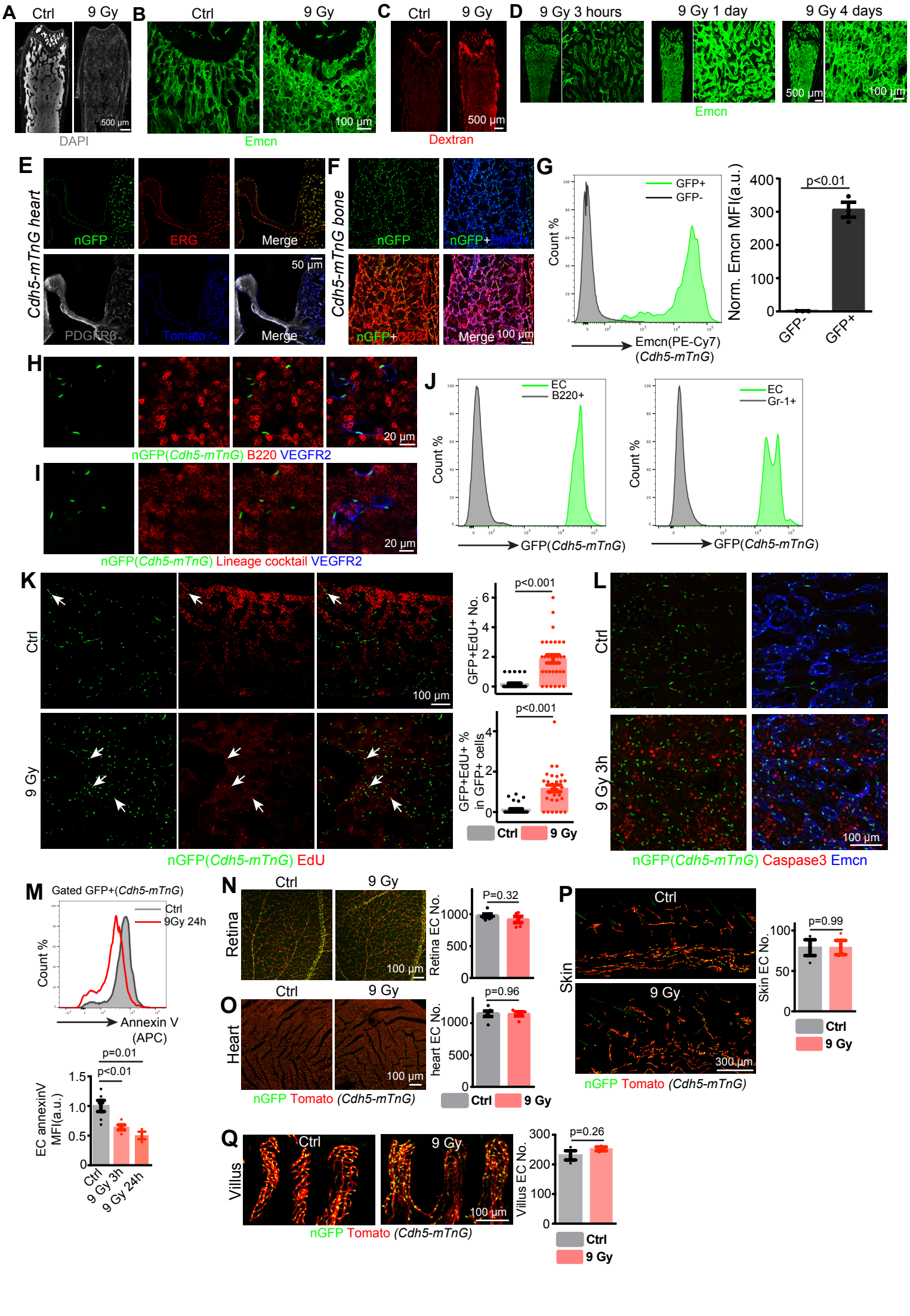
A
Ctrl
9 Gy
500 μm
DAPI
B
Ctrl
9 Gy
100 μm
Emcn
C
Ctrl
9 Gy
500 μm
Dextran
D
9 Gy 3 hours
9 Gy 1 day
9 Gy 4 days
500 μm
100 μm
Emcn
E
Cdh5-mTnG heart
nGFP
ERG
Merge
50 μm
PDGFRβ
Tomato
Merge
F
Cdh5-mTnG bone
nGFP
nGFP+EMCN
nGFP+CD31
Merge
100 μm
G
GFP+
GFP-
Count %
Emcn(PE-Cy7)
(Cdh5-mTnG)
Norm. Emcn MFI(a.u.)
p<0.01
400
300
200
100
0
GFP-
GFP+
H
20 μm
nGFP(Cdh5-mTnG) B220 VEGFR2
I
20 μm
nGFP(Cdh5-mTnG) Lineage cocktail VEGFR2
J
EC
B220+
Count %
GFP(Cdh5-mTnG)
EC
Gr-1+
Count %
GFP(Cdh5-mTnG)
K
Ctrl
9 Gy
100 μm
p<0.001
GFP+EdU+ No.
6
4
2
0
p<0.001
GFP+EdU+ % in GFP+ cells
4
2
0
Ctrl
9 Gy
nGFP(Cdh5-mTnG) EdU
L
Ctrl
9 Gy 3h
100 μm
nGFP(Cdh5-mTnG) Caspase3 Emcn
M
Gated GFP+(Cdh5-mTnG)
Ctrl
9Gy 24h
Count %
Annexin V
(APC)
p=0.01
p<0.01
EC annexinV MFI(a.u.)
1.5
1.0
0.5
0
Ctrl
9 Gy 3h
9 Gy 24h
N
Retina
Ctrl
9 Gy
100 μm
P=0.32
Retina EC No.
1000
500
0
O
Heart
Ctrl
9 Gy
100 μm
p=0.96
heart EC No.
1000
500
0
Ctrl
9 Gy
nGFP Tomato (Cdh5-mTnG)
P
Skin
Ctrl
9 Gy
300 μm
p=0.99
Skin EC No.
100
50
0
Ctrl
9 Gy
nGFP Tomato (Cdh5-mTnG)
Q
Villus
Ctrl
9 Gy
100 μm
p=0.26
Villus EC No.
300
200
100
0
Ctrl
9 Gy
nGFP Tomato (Cdh5-mTnG)

Figure S1. Irradiation induced other changes to bone vasculature, related to Figure 1

(A-B) DAPI labelled (A) and Emcn-immunostained (B) sections from control or lethally irradiated bone (9 Gy; 7 days post irradiation). The overview images are stitched from several individual z-stacked images.
(C) Representative images showing extravasation of intravenously injected Texas red-coupled Dextran (red) in control bone and 7 days post lethal irradiation (9 Gy). The overview images are stitched from several individual z-stacked images.
(D) Confocal overview and high-magnification images of diaphyseal vessels at 3 hours, 1 day and 4 days after lethal irradiation (9 Gy). Green: Emcn. The overview images are stitched from several individual z-stacked images.
(E) Validation of overlap between nuclear GFP (nGFP, green) signal and ERG immunostaining (red) in sections from P6 Cdh5-mTnG hearts.
(F) EC labelling in P6 Cdh5-mTnG bone.
(G) Flow cytometry validating Emcn expression in GFP+ cells from Cdh5-mTnG mice. Representative histogram of Emcn expression in GFP- or GFP+ cells and quantification of normalized mean fluorescence intensity (MFI). n=3 in each group. Error bars, mean± s.e.m. P values, two-tailed unpaired Student's t-Test.
(H) Representative images showing no overlap of nuclear GFP signal (green) in B220+ (red) hematopoietic cells.
(I) Representative images showing no overlap of nuclear GFP signal (Green) in lineage committed (red) hematopoietic cells.
(J) Representative FACS histogram showing clear separation of B220+ cells (or Gr-1+) and GFP+ cells in Cdh5-mTnG mice
(K) Representative single-plane images showing co-localization of EdU signal and nuclear GFP signal in Ctrl or irradiated (9 Gy 7 days) Cdh5-mTnG mice. About 40mg/kg EdU was injected at 7 consecutive days. Quantification for number and ratio of GFP+EdU+ signals in ctrl or irradiated Cdh5-mTnG mice (Ctrl=30 planes, 10 random planes/mouse; 9 Gy=30 planes, 10 random planes/mouse). Error bars, mean± s.e.m. P values, two-tailed unpaired Student's t-Test.
(L) Representative images showing expression of active caspase 3 in Ctrl and irradiated (9 Gy 3 hours) Cdh5-mTnG mice. Green, nGFP; red, active caspase 3; blue: Emcn.
(M) Representative histogram of Annexin V staining of Ctrl and irradiated (9 Gy 24 hours) ECs (GFP+) isolated from Cdh5-mTnG mice. Quantification of mean fluorescence intensity (MFI) of Annexin V signal (Ctrl n=6; 9Gy 3h n=5; 9Gy 24h n=3). Error bars, mean± s.e.m. P values, two-tailed unpaired Student's t-Test.
(N) Confocal images of retinal vessels at 7 days after irradiation. Quantification of GFP+ cells per image field (Ctrl n=6 mice; 9 Gy n=5 mice). Error bars, mean± s.e.m. P values, two-tailed unpaired Student's t-Test.
(O) Confocal images of heart vasculature in left ventricle at 7 days after irradiation. Quantification of GFP+ cells per image field (Ctrl n=6 mice; 9 Gy n=5 mice).
Error bars, mean± s.e.m. P values, two-tailed unpaired Student's t-Test. The overview images are stitched from several individual z-stacked images.
(P and Q) Confocal images of dermal vessels (P) and small intestinal villi (Q) at 7 days after irradiation. Quantification of GFP+ cells per image field (Ctrl n=3 mice; 9 Gy n=3 mice). Error bars, mean± s.e.m. P values, two-tailed unpaired Student's t-Test. The overview images are stitched from several individual z-stacked images.

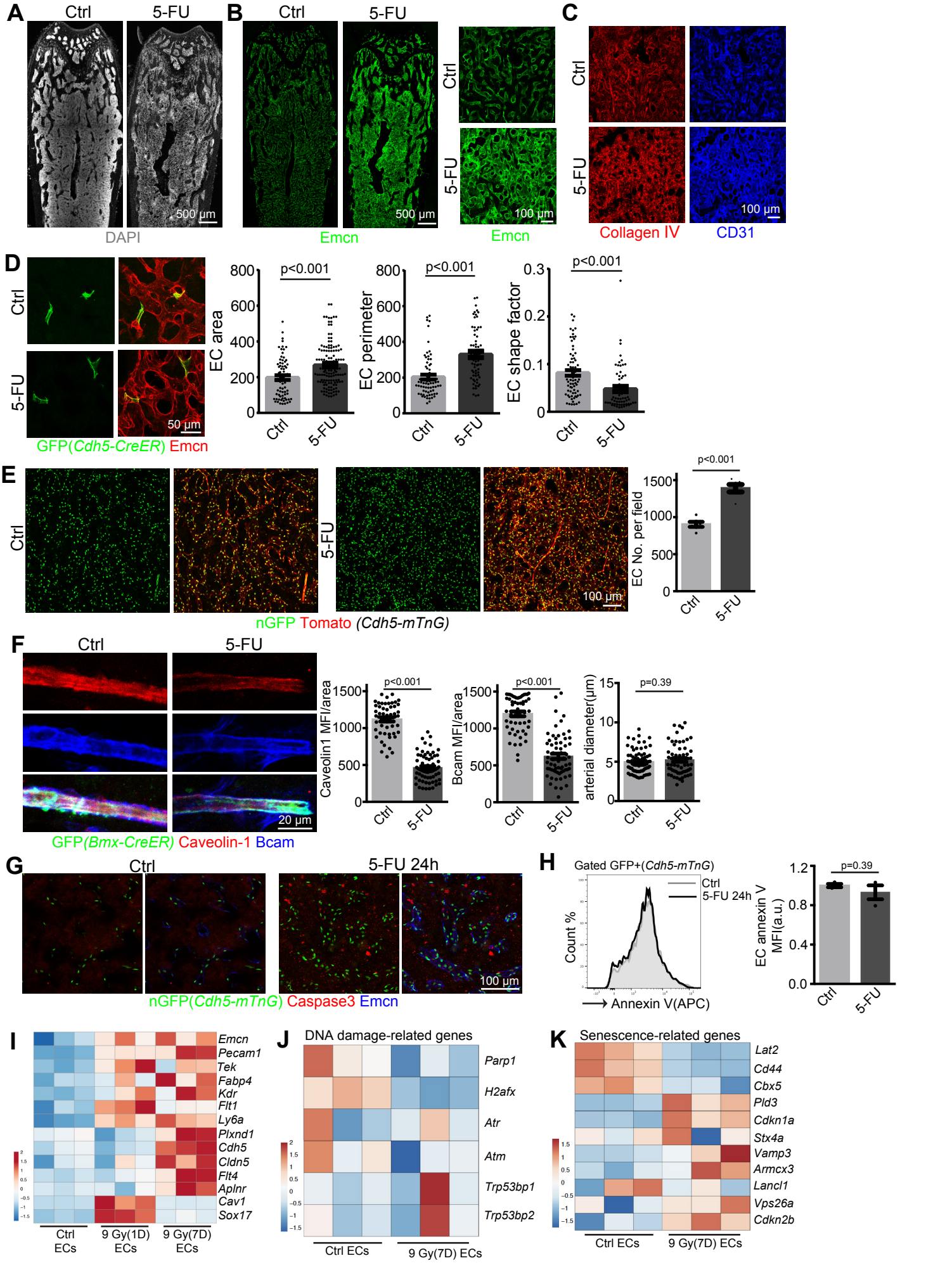
A
Ctrl
5-FU
500 μm
DAPI
B
Ctrl
5-FU
500 μm
Emcn
Ctrl
5-FU
100 μm
Emcn
C
Ctrl
5-FU
100 μm
Collagen IV
CD31
D
Ctrl
5-FU
50 μm
GFP(Cdh5-CreER) Emcn
EC area
p<0.001
EC perimeter
p<0.001
EC shape factor
p<0.001
E
Ctrl
5-FU
100 μm
nGFP Tomato (Cdh5-mTnG)
EC No. per field
p<0.001
F
Ctrl
5-FU
20 μm
GFP(Bmx-CreER) Caveolin-1 Bcam
Caveolin1 MFI/area
p<0.001
Bcam MFI/area
p<0.001
arterial diameter(μm)
p=0.39
G
Ctrl
5-FU 24h
100 μm
nGFP(Cdh5-mTnG) Caspase3 Emcn
H
Gated GFP+(Cdh5-mTnG)
Ctrl
5-FU 24h
Count %
Annexin V(APC)
EC annexin V MFI(a.u.)
p=0.39
I
Emcn
Pecam1
Tek
Fabp4
Kdr
Flt1
Ly6a
Plxnd1
Cdh5
Cldn5
Flt4
Aplnr
Cav1
Sox17
Ctrl ECs
9 Gy(1D) ECs
9 Gy(7D) ECs
J
DNA damage-related genes
Parp1
H2afx
Atr
Atm
Trp53bp1
Trp53bp2
Ctrl ECs
9 Gy(7D) ECs
K
Senescence-related genes
Lat2
Cd44
Cbx5
Pld3
Cdkn1a
Stx4a
Vamp3
Armcx3
Lancl1
Vps26a
Cdkn2b
Ctrl ECs
9 Gy(7D) ECs

Figure S2. Transcriptional changes in irradiated ECs and effect of 5-fluorouracil (5-FU) in bone vasculature, related to Figure 2

(A and B) Projected DAPI (white) and Emcn (green) staining in adult bone vasculature 7 days after 5-FU treatment. The overview images are stitched from several individual z-stacked images.
(C) High magnification confocal images of collagen IV (red) and CD31 (blue) in adult bone vasculature 7 days after 5-FU treatment.
(D) Maximum intensity projections showing morphology of ECs at single cell level in Cdh5-CreER R26-mTmG mice 7 days after 5-FU treatment. Tamoxifen was injected 6 days after 5-FU treatment. Quantification of area, perimeter and shape factor of 73 single ECs from 3 control mice and 67 single ECs from 3 5-FU-treated mice. Error bars, mean± s.e.m. P values, two-tailed unpaired Student's t-Test.
(E) Representative images and quantification of GFP+ cells in one image field of diaphysis in Cdh5-mT-nG mice 7 days after 5-FU treatment. n=6 in each group. Error bars, mean± s.e.m. P values, two-tailed unpaired Student's t-Test.
(F) Representative images and quantification of arterial vessels in Bmx-CreER R26-mTmG mice 7 days after 5-FU treatment. GFP(Green), Caveolin-1 (red) and Bcam (blue). Quantification of arterial vessel diameter (Ctrl=75 from 4 mice, 5-FU=63 from 4 mice), mean fluorescence intensity of caveolin-1 (Ctrl=54 from 4 mice, 5-FU=65 from 4 mice) and Bcam (Ctrl=54 from 4 mice, 5-FU=65 from 4 mice). Error bars, mean± s.e.m. P values, two-tailed unpaired Student's t-Test.
(G) Representative confocal images showing expression of active caspase 3 in Ctrl and 5-FU-treated Cdh5-mTnG mice at 24 hours after treatment. Green, nGFP; red, active caspase 3; blue: Emcn.
(H) Annexin V staining of Ctrl and 5-FU-treated (5-FU 24 hours) ECs (GFP+) from Cdh5-mTnG mice. Quantification of mean fluorescence intensity (MFI) of Annexin V signal (Ctrl n=3; 5-FU 24h n=3). Error bars, mean± s.e.m. P values, two-tailed unpaired Student's t-Test.
(I) Heatmap showing dynamic change of selected EC marker genes at the indicated times after irradiation.
(J and K) Heatmaps showing selected genes related to DNA damage (J) or senescence (K) after irradiation.

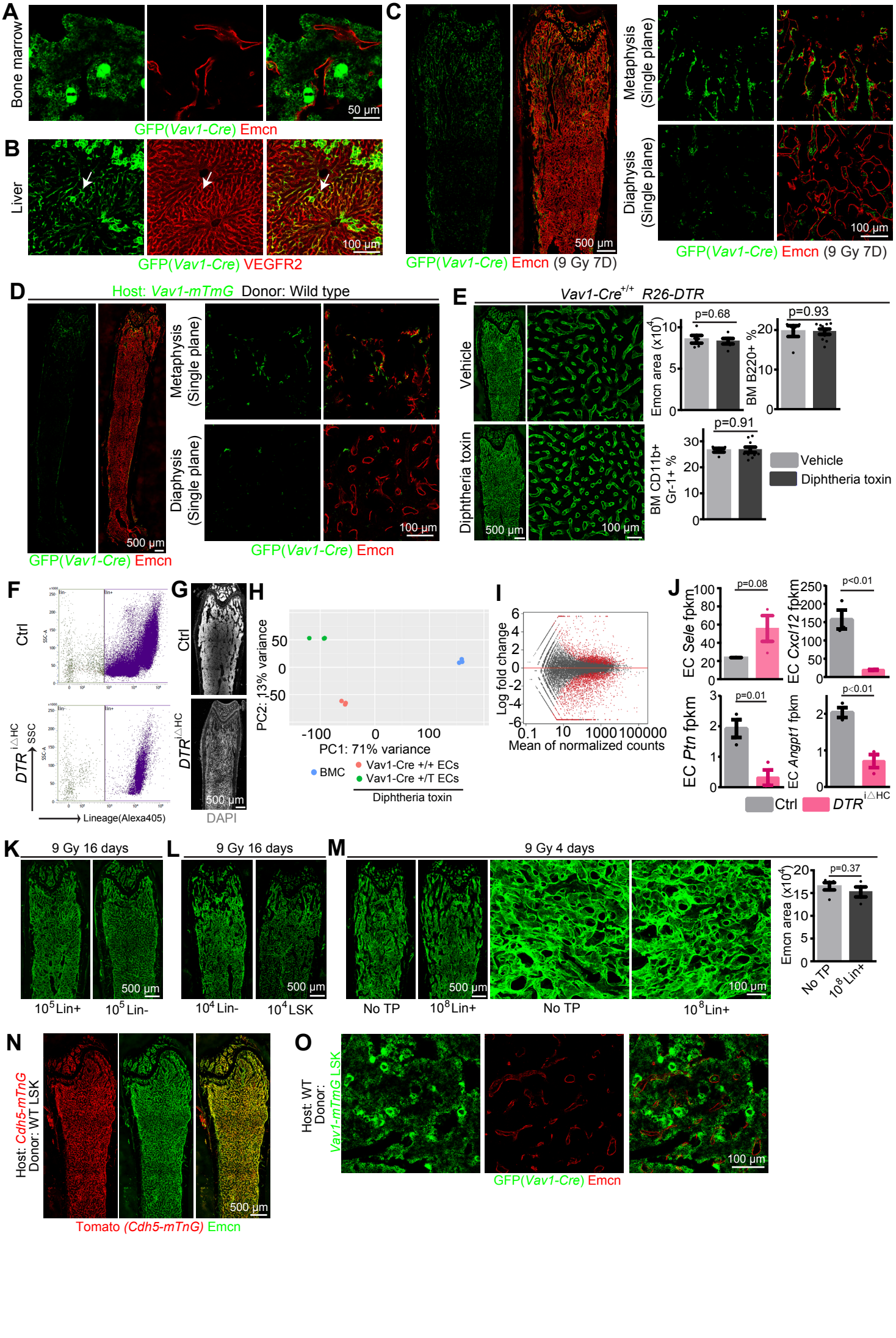
A
Bone marrow
50 μm
GFP(Vav1-Cre) Emcn
B
Liver
100 μm
GFP(Vav1-Cre) VEGFR2
C
500 μm
GFP(Vav1-Cre) Emcn (9 Gy 7D)
Metaphysis (Single plane)
Diaphysis (Single plane)
100 μm
GFP(Vav1-Cre) Emcn (9 Gy 7D)
D
Host: Vav1-mTmG Donor: Wild type
500 μm
GFP(Vav1-Cre) Emcn
Metaphysis (Single plane)
Diaphysis (Single plane)
100 μm
GFP(Vav1-Cre) Emcn
E
Vav1-Cre+/+ R26-DTR
Vehicle
Diphtheria toxin
500 μm
100 μm
Emcn area (x10^4)
p=0.68
BM B220+ %
p=0.93
BM CD11b+ Gr-1+ %
p=0.91
Vehicle
Diphtheria toxin
F
Ctrl
DTR i△HC
SSC
Lineage(Alexa405)
G
Ctrl
DTR i△HC
500 μm
DAPI
H
PC2: 13% variance
PC1: 71% variance
BMC
Vav1-Cre +/+ ECs
Vav1-Cre +/T ECs
Diphtheria toxin
I
Log fold change
Mean of normalized counts
J
EC Sele fpkm
p=0.08
EC Cxcl12 fpkm
p<0.01
EC Ptn fpkm
p=0.01
EC Angpt1 fpkm
p<0.01
Ctrl
DTR i△HC
K
9 Gy 16 days
500 μm
10^5 Lin+
10^5 Lin-
L
9 Gy 16 days
500 μm
10^4 Lin-
10^4 LSK
M
9 Gy 4 days
500 μm
No TP
10^8 Lin+
100 μm
No TP
10^8 Lin+
Emcn area (x10^4)
p=0.37
No TP
10^8 Lin+
N
Host: Cdh5-mTnG
Donor: WT LSK
500 μm
Tomato (Cdh5-mTnG) Emcn
O
Host: WT
Donor: Vav1-mTmG LSK
100 μm
GFP(Vav1-Cre) Emcn

Figure S3. Characterization of DTR$^{i\Delta HC}$ model, related to Figure 3

(A) Representative images showing no overt co-localization of Emcn+ ECs and GFP signal in Vav1-Cre R26-mTmG BM under steady-state conditions.
(B) Representative images showing co-localization (arrow) of VEGFR2 and GFP signals in Vav1-Cre R26-mTmG liver. The overview images are stitched from several individual z-stacked images.
(C and D) Overview and high-magnification (single plane) images showing Emcn and GFP signals in metaphysis and diaphysis of Vav1-Cre R26-mTmG mice at 7 days after 9 Gy irradiation without transplantation (C) and after transplantation of wild-type Lin- cells (D). Green, GFP; red, Emcn. The overview images are stitched from several individual z-stacked images.
(E) Diphtheria toxin injection in Cre- mice does not influence vessels and hematopoietic cells. Overview and high-magnification image and quantification of bone vessels (Emcn, green) after administration of diphtheria toxin (n=6) or vehicle control (n=5) in Vav1-Cre+/+ R26-DTR mice. The overview images are stitched from several individual z-stacked images. FACS quantification of B220+ B-lymphocytes and CD11b+ Gr-1+ myeloid cells percentage after administration of diphtheria toxin (n=10) or vehicle control (n=5) in Vav1-Cre+/+ R26-DTR mice. Error bars, mean± s.e.m. P values, two-tailed unpaired Student's t-Test.
(F) Representative FACS plots of Lin- and Lin+ cells 4 days after diphtheria toxin injection in littermate control (Vav1-Cre+/+ R26-DTR) and DTR$^{i\Delta HC}$ mice.
(G) Projected overview image of DAPI (white) signal 4 days after diphtheria toxin injection in littermate control (Vav1-Cre+/+ R26-DTR) and DTR$^{i\Delta HC}$ mice. The overview images are stitched from several individual z-stacked images.
(H) Principal component analysis of EC gene expression in DTR$^{i\Delta HC}$ and littermate control mice. DTA was injected into both DTR$^{i\Delta HC}$ and control mice, and ECs were isolated 4 days later.
(I) MA plot indicating differentially expressed genes in DTR$^{i\Delta HC}$ and control ECs 4 days after DTA injection.
(J) Quantification of selected HSC-related niche genes from RNA-seq analysis of DTR$^{i\Delta HC}$ and control ECs. N=3 per group, error bars, mean± s.e.m. P values, two-tailed unpaired Student's t-Test.
(K and L) Overview of Emcn-stained bone vasculature 16 days after irradiation and transplantation of $4x10^5$ Lin- or Lin+ cells (K) or of $2x10^4$ Lin- or LSK cells (L). The overview images are stitched from several individual z-stacked images.
(M) Overview and high-magnification confocal images of Emcn-stained bone vasculature 4 days after irradiation in mice without transplantation (No TP) or after transplantation with $1x10^8$ Lin+ cells. The overview images are stitched from several individual z-stacked images. Quantification of Emcn area (No TP n=5; 10^8 Lin+ n=4). Error bars, mean± s.e.m. P values, two-tailed unpaired Student's t-Test.
(N) Overview images of femur from Cdh5-mTnG recipient (9 Gy 16 days) transplanted with wildtype LSK cells. The overview images are stitched from several individual z-stacked images. Most of Emcn+ BM vessels (green) co-localize with tomato (red) signal of the Cdh5-mTnG reporter.
(O) High-magnification image showing wild-type recipient (9 Gy 16 days) transplanted with LSK cells from Vav1-mTmG donor. Emcn+ vessels (red) show no overt co-localization with GFP signal (green).

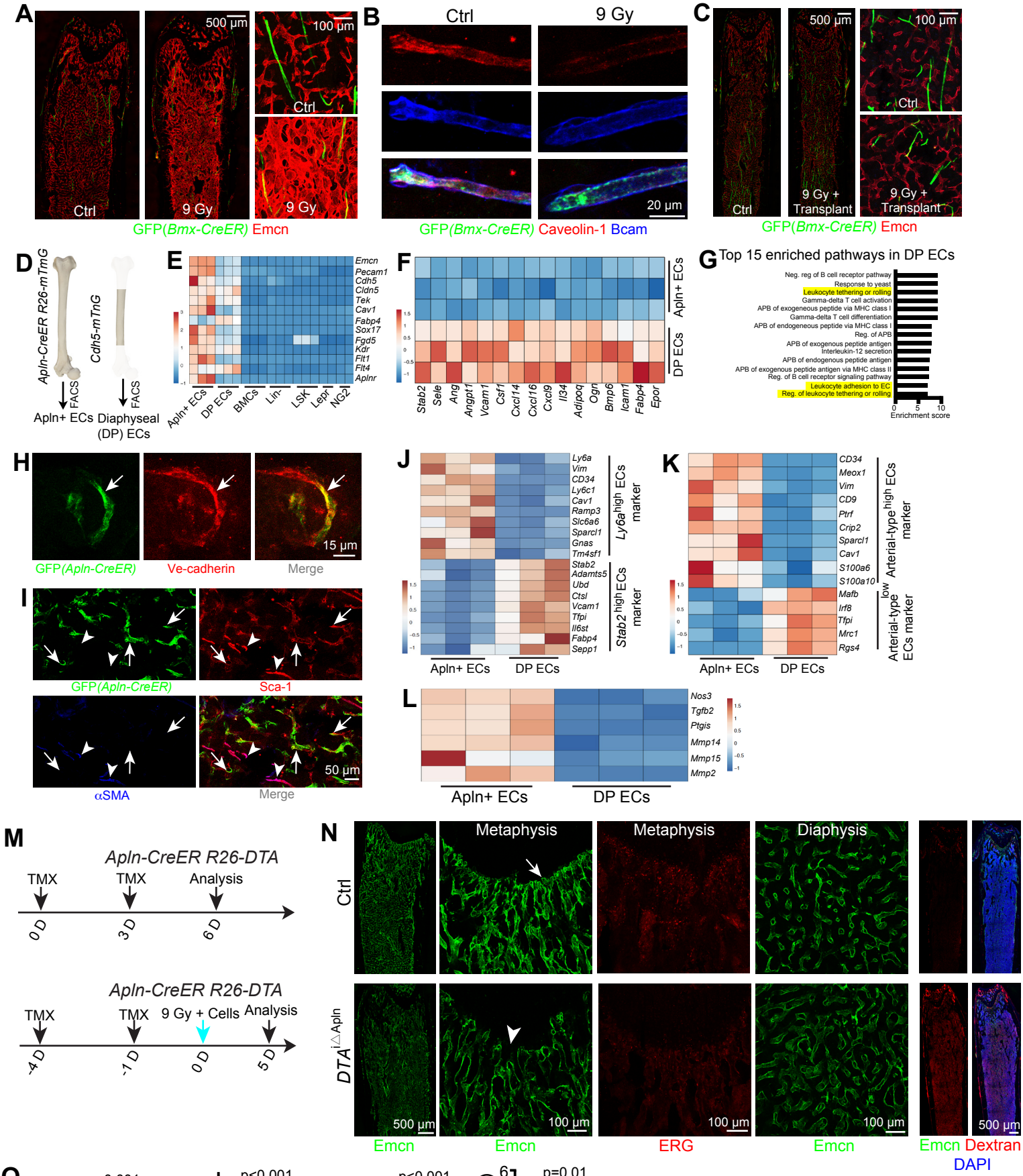
A
500 μm
100 μm
Ctrl
9 Gy
9 Gy
GFP(Bmx-CreER) Emcn
B
Ctrl
9 Gy
20 μm
GFP(Bmx-CreER) Caveolin-1 Bcam
C
500 μm
100 μm
Ctrl
9 Gy + Transplant
9 Gy + Transplant
GFP(Bmx-CreER) Emcn
D
Apln-CreER R26-mTmG
Cdh5-mTmG
FACS
FACS
Apln+ ECs
Diaphyseal (DP) ECs
E
Emcn
Pecam1
Cdh5
Cldn5
Tek
Cav1
Fabp4
Sox17
Fgd5
Kdr
Flt1
Flt4
Aplnr
Apln+ ECs
DP ECs
BMCs
Lin-
LSK
Lepr
NG2
F
Apln+ ECs
DP ECs
Stab2
Sele
Ang
Angpt1
Vcam1
Csf1
Cxcl14
Cxcl16
Cxcl9
Il34
Adipoq
Ogn
Bmp6
Icam1
Fabp4
Epor
G
Top 15 enriched pathways in DP ECs
Neg. reg of B cell receptor pathway
Response to yeast
Leukocyte tethering or rolling
Gamma-delta T cell activation
APB of exogeneous peptide via MHC class I
Gamma-delta T cell differentiation
APB of endogeneous peptide via MHC class I
Reg. of APB
APB of exogenous peptide antigen
Interleukin-12 secretion
APB of endogenous peptide antigen
APB of exogenous peptide antigen via MHC class II
Reg. of B cell receptor signaling pathway
Leukocyte adhesion to EC
Reg. of leukocyte tethering or rolling
0
5
10
Enrichment score
H
15 μm
GFP(Apln-CreER)
Ve-cadherin
Merge
I
GFP(Apln-CreER)
Sca-1
50 μm
αSMA
Merge
J
Ly6a
Vim
CD34
Ly6c1
Cav1
Ramp3
Slc6a6
Sparcl1
Gnas
Tm4sf1
Stab2
Adamts5
Ubd
Ctsl
Vcam1
Tfpi
Il6st
Fabp4
Sepp1
Ly6a high ECs marker
Stab2 high ECs marker
Apln+ ECs
DP ECs
K
CD34
Meox1
Vim
CD9
Ptrf
Crip2
Sparcl1
Cav1
S100a6
S100a10
Mafb
Irf8
Tfpi
Mrc1
Rgs4
Arterial-type high ECs marker
Arterial-type low ECs marker
Apln+ ECs
DP ECs
L
Nos3
Tgfb2
Ptgis
Mmp14
Mmp15
Mmp2
Apln+ ECs
DP ECs
M
Apln-CreER R26-DTA
TMX
TMX
Analysis
0 D
3 D
6 D
Apln-CreER R26-DTA
TMX
TMX
9 Gy + Cells
Analysis
-4 D
-1 D
0 D
5 D
N
Ctrl
DTA iΔApln
Metaphysis
Metaphysis
Diaphysis
500 μm
100 μm
100 μm
100 μm
500 μm
Emcn
Emcn
ERG
Emcn
Emcn Dextran
DAPI
O
MP bulge No./mm
p<0.001
ERG No. in MP
p<0.001
DP Diameter(μm)
p<0.001
Dextran area(x10^6)
p=0.01
Ctrl
DTA iΔApln

Figure S4. Characterization of Apln+ ECs and vascular defects in DTA$^{i\Delta Apln}$ in bone, related to Figure 4

(A) Overview and high magnification confocal images of Emcn+ (red) capillaries and GFP+ (green) arteries in Bmx-CreERT2 R26-mTmG mice at 7 days after lethal irradiation (9 Gy). The overview images are stitched from several individual z-stacked images.
(B) Representative images of arterial vessels in Bmx-CreER R26-mTmG mice 7 days after irradiation. GFP (green), Caveolin-1 (red) and Bcam (blue).
(C) Overview and high magnification confocal images of Emcn+ (red) capillaries and GFP+ (green) arteries in Bmx-CreERT2 R26-mTmG mice at 3 weeks after lethal irradiation and BM transplantation. The overview images are stitched from several individual z-stacked images.
(D) Schematic diagram depicting the isolation of Apln+ ECs from Apln-mTmG whole bone and of Cdh5-mTnG diaphyseal ECs.
(E) Heatmap showing the enrichment of selected endothelial marker genes in Apln+ ECs and diaphyseal (DP) ECs relative to bone marrow cells (BMCs), Lin- cells, LSK cells, and Lepr+ and NG2+ perivascular cells.
(F) Heatmap showing enrichment of specific niche-related genes in diaphyseal ECs relative to Apln+ ECs.
(G) GO biological signaling pathway analysis indicating the top 15 enriched signaling pathways in diaphyseal ECs.
(H) High magnification image showing VE-cadherin immunosignal (red) in Apln+ ECs (arrow) in Apln-mTmG mice.
(I) Apln+ ECs (green) in Apln-mTmG mice express Sca-1 (red, arrows) but are not covered by αSMA+ vSMCs (blue, arrowheads). The overview images are stitched from several individual z-stacked images.
(J) Heatmap showing expression of Ly6a^{high} ECs and Stab2^{high} ECs markers in Apln+ ECs and diaphyseal ECs (Tikhonova et al., 2019).
(K) Heatmap showing expression of “arterial-type” EC markers in Apln+ ECs but not diaphyseal ECs (Baryawno et al., 2019).
(L) Heatmap showing expression pattern of selected anti-inflammatory genes in Apln+ ECs and diaphyseal ECs.
(M) Experimental protocol for DTA-mediated ablation of Apln+ ECs under physiological conditions (top) or in combination with irradiation and transplantation of DTA$^{i\Delta Apln}$ recipients.
(N) Confocal overview and high-magnification images of Emcn (green) and ERG (red) stained vessels in metaphsis and diaphysis of adult control and DTA$^{i\Delta Apln}$ mice. Arrows indicated EC bulbs near control (Ctrl) growth plate and arrowheads mark local vessel lesions in DTA$^{i\Delta Apln}$ samples. Confocal overview image of Emcn (green), extravasation dextran (red) and DAPI (blue) stained BM of adult DTA$^{i\Delta Apln}$ and control mice. The overview images are stitched from several individual z-stacked images.
(O) Quantification of vessel buds (ctrl=6, DTA$^{i\Delta Apln}$=6) and ERG+ cells (ctrl=5 , DTA$^{i\Delta Apln}$ =5) in metaphysis, diameter of diaphyseal vessels (ctrl=6 , DTA$^{i\Delta Apln}$ =6), dextran leakage area (ctrl=3 , DTA$^{i\Delta Apln}$ =4). Error bars, mean± s.e.m. P values, two-tailed unpaired Students’ t-Test.

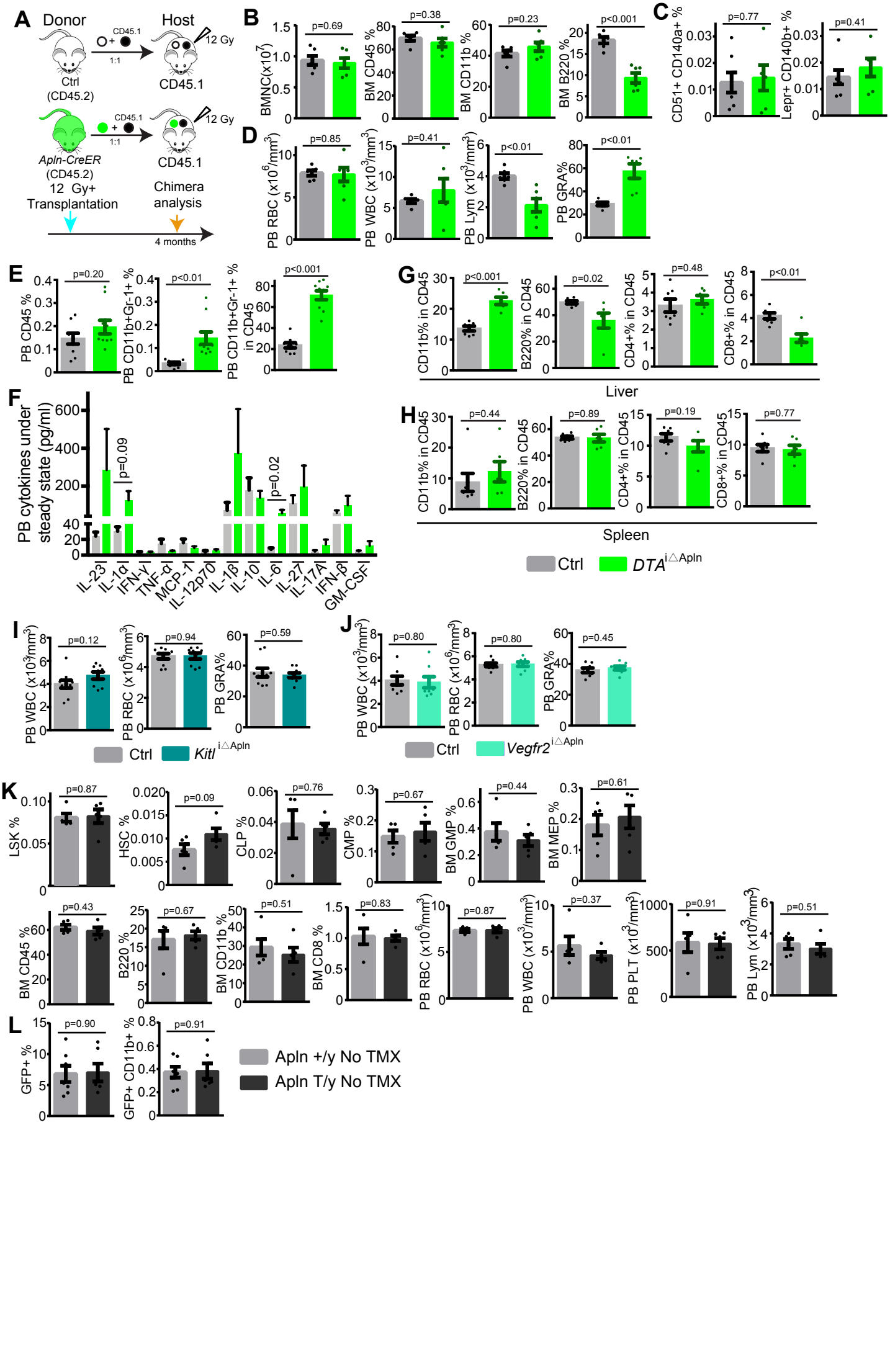
A
Donor
Host
CD45.1
1:1
12 Gy
Ctrl
(CD45.2)
CD45.1
Apln-CreER
(CD45.2)
12 Gy+
Transplantation
Chimera
analysis
4 months
B
BMNC(x10^7)
BM CD45 %
BM CD11b %
BM B220 %
p=0.69
p=0.38
p=0.23
p<0.001
C
CD51+ CD140a+ %
Lepr+ CD140b+ %
p=0.77
p=0.41
D
PB RBC (x10^6/mm^3)
PB WBC (x10^3/mm^3)
PB Lym (x10^3/mm^3)
PB GRA%
p=0.85
p=0.41
p<0.01
p<0.01
E
PB CD45 %
PB CD11b+Gr-1+ %
PB CD11b+Gr-1+ % in CD45
p=0.20
p<0.01
p<0.001
G
CD11b% in CD45
B220% in CD45
CD4+% in CD45
CD8+% in CD45
p<0.001
p=0.02
p=0.48
p<0.01
Liver
F
PB cytokines under steady state (pg/ml)
p=0.09
p=0.02
IL-23
IL-1α
IFN-γ
TNF-α
MCP-1
IL-12p70
IL-1β
IL-10
IL-6
IL-27
IL-17A
IFN-β
GM-CSF
H
CD11b% in CD45
B220% in CD45
CD4+% in CD45
CD8+% in CD45
p=0.44
p=0.89
p=0.19
p=0.77
Spleen
Ctrl
DTA^iΔApln
I
PB WBC (x10^3/mm^3)
PB RBC (x10^6/mm^3)
PB GRA%
p=0.12
p=0.94
p=0.59
Ctrl
Kitl^iΔApln
J
PB WBC (x10^3/mm^3)
PB RBC (x10^6/mm^3)
PB GRA%
p=0.80
p=0.80
p=0.45
Ctrl
Vegfr2^iΔApln
K
LSK %
HSC %
CLP %
CMP %
BM GMP %
BM MEP %
p=0.87
p=0.09
p=0.76
p=0.67
p=0.44
p=0.61
BM CD45 %
B220 %
BM CD11b %
BM CD8 %
PB RBC (x10^6/mm^3)
PB WBC (x10^3/mm^3)
PB PLT (x10^3/mm^3)
PB Lym (x10^3/mm^3)
p=0.43
p=0.67
p=0.51
p=0.83
p=0.87
p=0.37
p=0.91
p=0.51
L
GFP+ %
GFP+ CD11b+ %
p=0.90
p=0.91
Apln +/y No TMX
Apln T/y No TMX

Figure S5. Loss of Apln+ ECs but not of Apln expression causes hematopoietic defects under steady state, related to Figure 5.

(A) Schematic showing protocols for CD45.2/CD45.1 long-term repopulation assay for $DTA^{i\Delta Apln}$, $Kitl^{i\Delta Apln}$ and $Vegfr2^{i\Delta Apln}$ mice.
(B) Flow cytometric analysis of hematopoietic cell subpopulations in the $DTA^{i\Delta Apln}$ BM (n=6 in each group). Error bars, mean± s.e.m. P values, two-tailed unpaired Student's t-Test. BMNC, bone marrow nucleated cells;
(C) Percentage of perivascular cell subpopulations in $DTA^{i\Delta Apln}$ (n=6) and control (n=7) bone. Error bars, mean± s.e.m. P values, two-tailed unpaired Student's t-Test.
(D) Blood count analysis of $DTA^{i\Delta Apln}$ peripheral blood (PB) components (n=6 in each group). Error bars, mean± s.e.m. P values, two-tailed unpaired Student's t-Test. RBC, red blood cells; WBC, white blood cells; Lym, lymphocytes; GRA, granulocyte.
(E) FACS analysis of $DTA^{i\Delta Apln}$ peripheral blood (PB) components under steady state (Ctrl=9, $DTA^{i\Delta Apln}$=10). Error bars, mean± s.e.m. P values, two-tailed unpaired Student's t-Test.
(F) Cytokine levels in peripheral blood plasma of $DTA^{i\Delta Apln}$ mice under steady state. Cytokine level lower than detection limit was excluded from quantification. n=2-8 in each group. Error bars, mean± s.e.m. P values, two-tailed unpaired Student's t-Test. P values higher than 0.1 are not indicated.
(G and H) FACS analysis of $DTA^{i\Delta Apln}$ liver (G) and spleen (H) leukocytes under steady-state (Ctrl=7, $DTA^{i\Delta Apln}$ =6). Error bars, mean± s.e.m. P values, two-tailed unpaired Student's t-Test.
(I) Blood count analysis of $Kitl^{i\Delta Apln}$ peripheral blood (PB) components (Ctrl=10; $Kitl^{i\Delta Apln}$ =9). Error bars, mean± s.e.m. P values, two-tailed unpaired Student's t-Test. WBC, white blood cells; RBC, red blood cells; GRA, granulocyte.
(J) Blood count analysis of $Vegfr2^{i\Delta Apln}$ peripheral blood (PB) components (Ctrl=8; $Vegfr2^{i\Delta Apln}$ =8). Error bars, mean± s.e.m. P values, two-tailed unpaired Student's t-Test. WBC, white blood cells; RBC, red blood cells; GRA, granulocyte.
(K) Flow cytometric analysis of hematopoietic cell subpopulations in Apln (T/y) and control bone marrow and peripheral blood (PB). Animals in this experiment were not treated with tamoxifen to evaluate the effect of the loss of Apln expression in Apln-CreERT knock-in males (equivalent to full knockout mice) (n=5 per group). Error bars, mean± s.e.m. P values, two-tailed unpaired Student's t-Test. CLP, common lymphoid progenitors; CMP, common myeloid progenitors; GMP, granulocyte-monocyte progenitors; MEP, Megakaryocyte-erythroid progenitors; RBC, red blood cells; WBC, white blood cells; PLT, platelets; Lym, lymphocytes.
(L) Flow cytometric analysis of hematopoietic reconstitution after loss of Apln expression in Apln-CreERT T/y knockout (n=6) and control males (n=7) without tamoxifen (TMX) administration. Vav1-Cre R26-mTmG hematopoietic cells were used as donors. Error bars, mean± s.e.m. P values, two-tailed unpaired Student's t-Test.

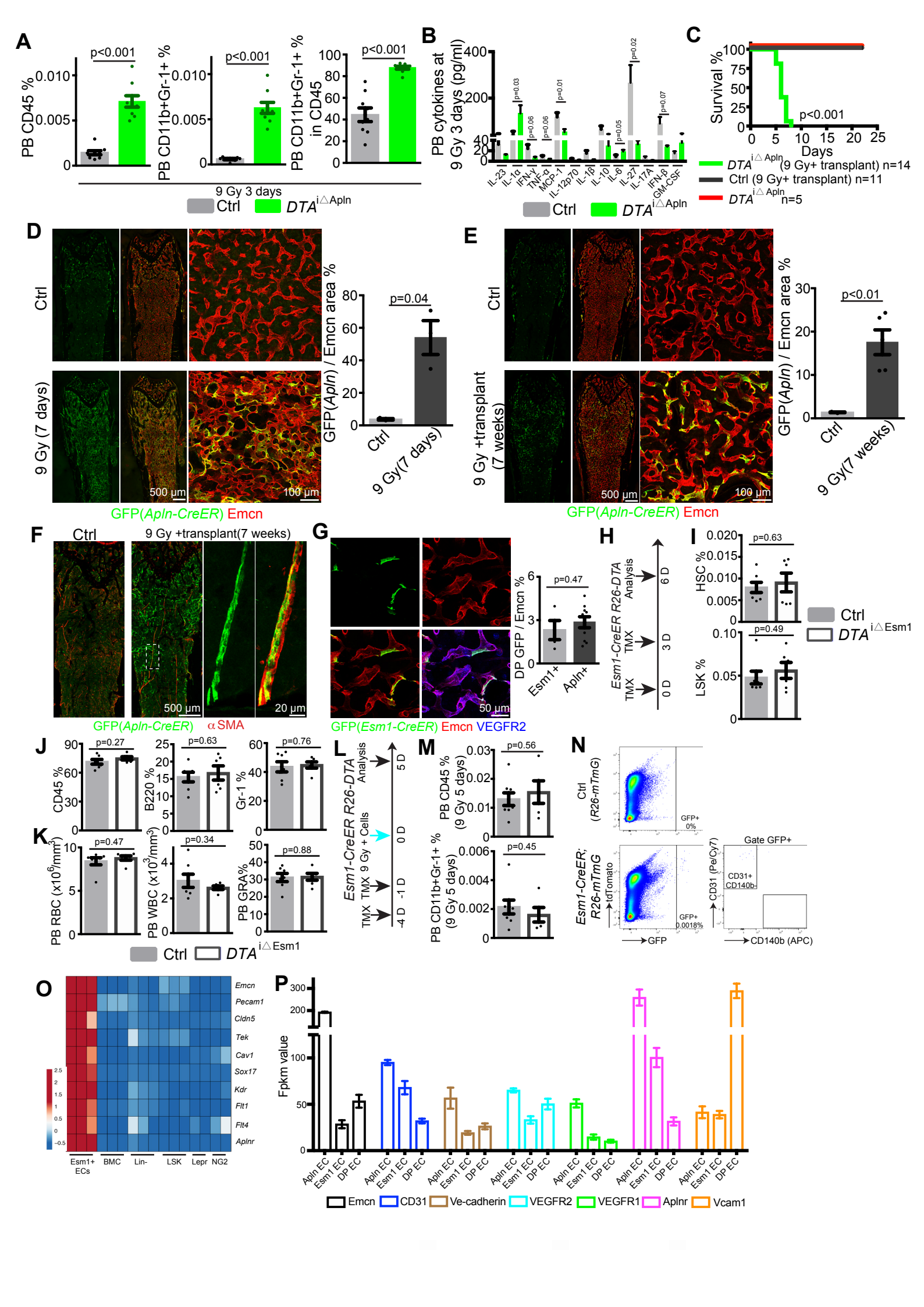
A
PB CD45 %
p<0.001
PB CD11b+Gr-1+ %
p<0.001
PB CD11b+Gr-1+ % in CD45
p<0.001
9 Gy 3 days
Ctrl
DTA iΔApln
B
PB cytokines at 9 Gy 3 days (pg/ml)
IL-23
IL-1α
IFN-γ
TNF-α
MCP-1
IL-12p70
IL-1β
IL-10
IL-6
IL-27
IL-17A
IFN-β
GM-CSF
Ctrl
DTA iΔApln
C
Survival %
p<0.001
Days
DTA iΔApln (9 Gy+ transplant) n=14
Ctrl (9 Gy+ transplant) n=11
DTA iΔApln n=5
D
Ctrl
9 Gy (7 days)
500 μm
100 μm
GFP(Apln) / Emcn area %
p=0.04
Ctrl
9 Gy(7 days)
GFP(Apln-CreER) Emcn
E
Ctrl
9 Gy +transplant (7 weeks)
500 μm
100 μm
GFP(Apln) / Emcn area %
p<0.01
Ctrl
9 Gy(7 weeks)
GFP(Apln-CreER) Emcn
F
Ctrl
9 Gy +transplant(7 weeks)
500 μm
20 μm
GFP(Apln-CreER) αSMA
G
50 μm
DP GFP / Emcn %
p=0.47
Esm1+
Apln+
GFP(Esm1-CreER) Emcn VEGFR2
H
Esm1-CreER R26-DTA
Analysis
TMX
TMX
6 D
3 D
0 D
I
HSC %
p=0.63
LSK %
p=0.49
Ctrl
DTA iΔEsm1
J
CD45 %
p=0.27
B220 %
p=0.63
Gr-1 %
p=0.76
K
PB RBC (x10^6/mm^3)
p=0.47
PB WBC (x10^3/mm^3)
p=0.34
PB GRA%
p=0.88
Ctrl
DTA iΔEsm1
L
Esm1-CreER R26-DTA
Analysis
9 Gy + Cells
TMX
TMX
5 D
0 D
-1 D
-4 D
M
PB CD45 % (9 Gy 5 days)
p=0.56
PB CD11b+Gr-1+ % (9 Gy 5 days)
p=0.45
N
Ctrl (R26-mTmG)
GFP+ 0%
Esm1-CreER; R26-mTmG
tdTomato
GFP+ 0.0018%
GFP
Gate GFP+
CD31+ CD140b-
CD31 (Pe/Cy7)
CD140b (APC)
O
Emcn
Pecam1
Cldn5
Tek
Cav1
Sox17
Kdr
Flt1
Flt4
Aplnr
Esm1+ ECs
BMC
Lin-
LSK
Lepr
NG2
P
Fpkm value
Apln EC
Esm1 EC
DP EC
Emcn
CD31
Ve-cadherin
VEGFR2
VEGFR1
Aplnr
Vcam1

Figure S6. Role of Apln+ ECs but not Esm1+ ECs in hematopoiesis and transplantation, related to Figure 6.

(A) FACS analysis of DTA$^{i\Delta Apln}$ peripheral blood (PB) components 3 days after irradiation and transplantation (Ctrl=9, DTA$^{i\Delta Apln}$ =9). Error bars, mean± s.e.m. P values, two-tailed unpaired Student's t-Test.
(B) Cytokine levels in peripheral blood plasma of DTA$^{i\Delta Apln}$ mice 3 days after irradiation and transplantation. Cytokine level lower than detection limit was excluded from quantification. n=2-8 in each group. Error bars, mean± s.e.m. P values, two-tailed unpaired Student's t-Test. P values higher than 0.1 are not indicated.
(C) Survival (in days) of DTA$^{i\Delta Apln}$ mutants (n=5) relative to irradiated (9 Gy) and transplanted control (Apln-CreER+/y, n=11) and DTA $^{i\Delta Apln}$ mice (n=14).
(D) Genetic lineage tracing of GFP+ cells in Apln-mTmG long bone at 8 days after a single 4-OHT administration with or without irradiation at day 2. Confocal overview images and magnification of diaphysis. The overview images are stitched from several individual z-stacked images. Quantification of GFP+ area relative to Emcn+ area in diaphysis (n=3 in each group). Error bars, mean± s.e.m. P values, two-tailed unpaired Student's t-Test.
(E) Genetic lineage tracing of GFP+ cells in Apln-mTmG long bone at 7 weeks after a single 4-OHT administration with or without irradiation and transplantation at day 2. Confocal overview images and magnification of diaphysis. The overview images are stitched from several individual z-stacked images. Quantification of GFP+ area relative to Emcn+ area in diaphysis (Ctrl=3; 9 Gy=5). Error bars, mean± s.e.m. P values, two-tailed unpaired Student's t-Test.
(F) Confocal overview images showing αSMA+ vSMCs and GFP signals in genetic lineage tracing experiments with Apln-mTmG at 7 weeks after irradiation and transplantation. The overview images are stitched from several individual z-stacked images. Dashed box and high magnified images show descendants of Apln+ ECs in association with vSMCs.
(G) Projected confocal image showing Esm1-CreER R26-mTmG mice with genetically labelled Esm1+ BM ECs. Green, GFP(Esm1-CreER); Red, Emcn; Blue, VEGFR2. Quantification of the percentages of Esm1+ ECs and Apln+ ECs in diaphysis (Esm1+ =4; Apln+ =10). Error bars, mean± s.e.m. P values, two-tailed unpaired Student's t-Test.
(H) Experimental protocol for DTA-mediated ablation of Esm1+ ECs under physiological conditions.
(I) Percentage of BM HSC and LSK cells in control (n=7) and DTAiΔEsm1 mice (n=6) under steady state conditions. Error bars, mean± s.e.m. P values, two-tailed unpaired Student's t-Test.
(J) Percentage of BM CD45+, B220+ and Gr-1+ cells in control (n=7) and DTA$^{i\Delta Esm1}$ mice (n=6) under steady state. Error bars, mean± s.e.m. P values, two-tailed unpaired Student's t-Test.
(K) Blood counts of BM RBC, WBC and GRA cells in control (n=7) and DTA$^{i\Delta Esm1}$ mice (n=6) under steady state. RBC, red blood cells; WBC, white blood cells, GRA, granulocyte. Error bars, mean± s.e.m. P values, two-tailed unpaired Student's t-Test.
(L) Experimental protocol for DTA-mediated ablation of Esm1+ ECs in combination with irradiation and transplantation of DTA $^{i\Delta Esm1}$ recipients.
(M) FACS analysis of CD45+ or CD11b+Gr-1+ cells in PB of control (n=8) and DTA$^{i\Delta Esm1}$ mice (n=5) 5 days after irradiation. Error bars, mean± s.e.m. P values, two-tailed unpaired Student's t-Test.
(N) Representative FACS plot showing gating strategy to isolate Esm1+ ECs (defined as GFP+CD31+CD140b-) from Esm1-mTmG mice.
(O) Heatmap of selective core EC markers genes showing significant enrichment of these genes in Esm1+ ECs relative to BM hematopoietic cells and mesenchymal cells.
(P) Expression levels of core EC marker genes in Apln+ ECs, Esm1+ ECs and total diaphyseal ECs (DP ECs) at transcript level based on RNA-seq data.

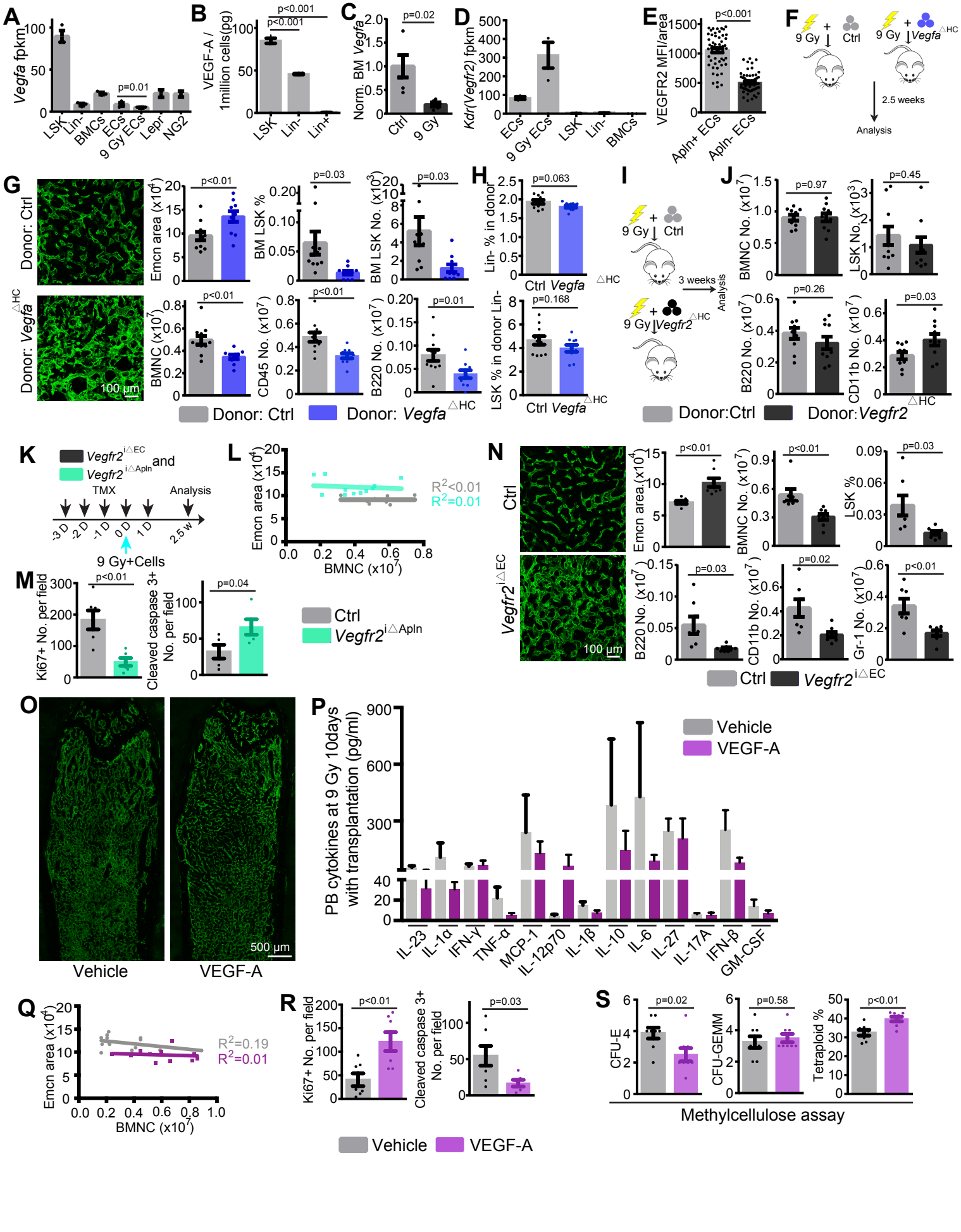
A
Vegfa fpkm
LSK
Lin-
BMCs
ECs
9 Gy ECs
Lepr
NG2
p=0.01
B
VEGF-A / 1million cells(pg)
p<0.001
p<0.001
LSK
Lin-
Lin+
C
Norm. BM Vegfa
p=0.02
Ctrl
9 Gy
D
Kdr(Vegfr2) fpkm
ECs
9 Gy ECs
LSK
Lin-
BMCs
E
VEGFR2 MFI/area
p<0.001
Apln+ ECs
Apln- ECs
F
9 Gy
Ctrl
9 Gy
Vegfa△HC
2.5 weeks
Analysis
G
Donor: Ctrl
Donor: Vegfa△HC
100 μm
Emcn area (x10⁴)
p<0.01
BM LSK %
p=0.03
BM LSK No. (x10³)
p=0.03
BMNC (x10⁷)
p<0.01
CD45 No. (x10⁷)
p<0.01
B220 No. (x10⁷)
p=0.01
△HC
Donor: Ctrl
Donor: Vegfa
H
Lin- % in donor
p=0.063
Ctrl
Vegfa
△HC
LSK % in donor Lin-
p=0.168
Ctrl
Vegfa
△HC
I
9 Gy
Ctrl
3 weeks
Analysis
9 Gy
Vegfr2△HC
J
BMNC No. (x10⁷)
p=0.97
LSK No. (x10³)
p=0.45
B220 No. (x10⁷)
p=0.26
CD11b No. (x10⁷)
p=0.03
△HC
Donor:Ctrl
Donor:Vegfr2
K
Vegfr2 i△EC and Vegfr2 i△Apln
TMX
Analysis
-3 D
-2 D
-1 D
0 D
1 D
2.5 w
9 Gy+Cells
L
Emcn area (x10⁴)
R²<0.01
R²=0.01
BMNC (x10⁷)
Ctrl
Vegfr2 i△Apln
M
Ki67+ No. per field
p<0.01
Cleaved caspase 3+ No. per field
p=0.04
N
Ctrl
Vegfr2 i△EC
100 μm
Emcn area (x10⁴)
p<0.01
BMNC No. (x10⁷)
p<0.01
LSK %
p=0.03
B220 No. (x10⁷)
p=0.03
CD11b No. (x10⁷)
p=0.02
Gr-1 No. (x10⁷)
p<0.01
Ctrl
Vegfr2 i△EC
O
500 μm
Vehicle
VEGF-A
P
PB cytokines at 9 Gy 10days with transplantation (pg/ml)
Vehicle
VEGF-A
IL-23
IL-1α
IFN-γ
TNF-α
MCP-1
IL-12p70
IL-1β
IL-10
IL-6
IL-27
IL-17A
IFN-β
GM-CSF
Q
Emcn area (x10⁴)
R²=0.19
R²=0.01
BMNC (x10⁷)
R
Ki67+ No. per field
p<0.01
Cleaved caspase 3+ No. per field
p=0.03
S
CFU-E
p=0.02
CFU-GEMM
p=0.58
Tetraploid %
p<0.01
Methylcellulose assay
Vehicle
VEGF-A

Figure S7. VEGFR2 in endothelial and hematopoietic cells have different functions during transplantation, related to Figure 7.

(A) RNA-seq data (fpkm values) of Vegfa in 7 different bone cell groups. n=3 for LSK, Lin-, BMCs, ECs, and irradiated (9 Gy) ECs; n=2 for Lepr+ and NG2+ perivascular cells(Asada et al., 2017). Error bars, mean± s.e.m. P values, two-tailed unpaired Student's t-Test.
(B) ELISA of cellular VEGF-A in LSK (n=3), Lin- (n=4) and Lin+ (n=4) subpopulations. Error bars, mean± s.e.m. P values, two-tailed unpaired Student's t-Test.
(C) RT-qPCR analysis of Vegfa levels in whole BM cells 7 days after irradiation or in controls without irradiation (n=5 per group). Error bars, mean± s.e.m. P values, two-tailed unpaired Student's t-Test.
(D) RNA-seq data (fpkm values) of Kdr/Vegfr2 in 5 different bone cell groups (n=3 each group). Error bars, mean± s.e.m.
(E) VEGFR2 expression at protein level (n=55 each group, from 3 mice) in Apln+ EC and non-Apln+ EC. Error bars, mean± s.e.m.
(F) Schematic diagram depicting the transplantation of Vegfa$^{\Delta HC}$ and littermate control Lin- ($3x10^5$) cells into irradiated wild-type recipients.
(G) Representative image of bone vasculature 2.5 weeks after irradiation and transplantation of $3x10^5$ Lin- cells derived from control or Vegfa$^{\Delta HC}$ donor mice. Graphs show Emcn area per field and BMNC number in recipient mice (control=11, Vegfa$^{\Delta HC}$ =10). Quantification of LSK, CD45+, and B220+ cell numbers and LSK percentage (control n=11, Vegfa$^{\Delta HC}$ n=10). Error bars, mean± s.e.m. P values, two-tailed unpaired Student's t-Test.
(H) Percentage of Lin- cells and percentage of LSK cells in Vegfa$^{\Delta HC}$ (n=10) and control (n=11) BM under steady state conditions.
(I) Schematic diagram depicting the transplantation of Vegfr2$^{\Delta HC}$ and control bone marrow cells into wild-type recipients.
(J) Flow cytometric analysis of BMNC number, LSK cell number, B220 cell number and CD11b cell number in recipients transplanted with Vegfr2$^{\Delta HC}$ or Ctrl donor cells (n=10 per group). Error bars, mean± s.e.m. P values, two-tailed unpaired Student's t-Test.
(K) Schematic depiction of the experimental protocol for the transplantation of Lin- ($3x10^5$) cells into Vegfr2$^{i\Delta EC}$ or Vegfr2$^{i\Delta Apln}$ recipient mice.
(L) Mathematical regression analysis showing the lack of correlation between BMNC number and Emcn+ area in Ctrl (grey, n=11) and Vegfr2$^{i\Delta Apln}$ (turquoise, n=11) samples. R^2, coefficient of determination, range from 0 to 1. R^2=1 means perfect fit of data points and equation.
(M) Quantification of Ki67+ (Ctrl=6; Vegfr2$^{i\Delta Apln}$ =6) and cleaved caspase 3+ (Ctrl=5; Vegfr2$^{i\Delta Apln}$=5) signal per image field in Ctrl and Vegfr2$^{i\Delta Apln}$ bone sections. Error bars, mean± s.e.m. P values, two-tailed unpaired Student's t-Test.
(N) Representative high magnification images of Emcn+ bone vasculature in transplanted Vegfr2$^{i\Delta EC}$ or control recipients. Quantification of Emcn+ area, BMNC number, LSK percentage, B220 cell number, CD11b cell number and Gr-1 cell number in Vegfr2$^{i\Delta EC}$ (n=8) or control recipients (n=7). Error bars, mean± s.e.m. P values, two-tailed unpaired Student's t-Test.
(O) Representative overview of Emcn+ bone vasculature in VEGF-A or vehicle control-treated recipient mice. The overview images are stitched from several individual z-stacked images.
(P) Cytokine levels in peripheral blood plasma of irradiated mice 10 days after transplantation together with VEGF-A infusion. Cytokine level lower than detection limit was excluded from quantification. N=4-6 in each group. Error bars, mean± s.e.m. P values, two-tailed unpaired Student's t-Test. P values higher than 0.1 are not indicated.
(Q) Mathematical regression analysis showing the lack of correlation between BMNC number and Emcn+ area in Ctrl (vehicle, n=14) and VEGF-A-treated bone samples (purple, n=11).
(R) Quantification of Ki67+ (Ctrl=7; VEGF-A=7) and cleaved caspase 3+ (Ctrl=7; VEGF-A=6) signal per image field in Ctrl and VEGF-A-treated bone sections. Error bars, mean± s.e.m. P values, two-tailed unpaired Student's t-Test.
(S) Quantification of CFU-E, CFU-GEMM number and percentage of cells in tetraploid state (4 nucleus,

Table S1. Summary of genetic mouse models used in this study.

Full Name	Short name	Inducible	Reporter	Purpose
Cdh5 membrane-Tdtomato H2B-EGFP	*Cdh5-mTnG*		H2B-GFP (nuclear) and mem-Tdtomato	Genetic labeling of ECs for imaging and FACS
Rosa26-mT/mG	*R26-mTmG*		Cre-induced switch from mem-Tomato to mem-GFP	Labeling of Cre-positive cells and their descendants
Cdh5(PAC)-CreERT2	*Cdh5-CreERT2*	Yes	-	Labeling of ECs and their descendants
Apln-CreERT2	-	Yes	-	Labeling of Apln+ ECs and their descendants
Bmx-CreERT2	-	Yes	-	Labeling of arterial ECs and their descendants
Vav1-Cre	-	No	-	Labeling and knockout of hematopoietic cells
VEGFa^{tm2Gne}	-		-	Conditional knockout of *Vegfa*
Kdr^{tm1Wag}	-		-	Conditional knockout of *Vegfr2/Kdr*
Rosa26-DTR	-		-	Conditional ablation of Cre+ cells, triggered by diphtheria toxin injection
Rosa26-DTA$^{tm1(DTA)Mrc}$	-		-	Conditional ablation of Cre+ cells, triggered by tamoxifen injection
Cdh5(PAC)-CreERT2 Rosa26-mT/mG	*Cdh5-mTmG*	Yes	mem-GFP after Cre recombination	Tamoxifen injection to label all ECs or cells at single cell level
Bmx-CreERT2 Rosa26-mT/mG	*Bmx-mTmG*	Yes	mem-GFP after Cre recombination	Labeling of arterial ECs and their descendants
Apln-CreERT2 Rosa26-mT/mG	*Apln-mTmG*	Yes	mem-GFP after Cre recombination	Labeling of Apln+ ECs and their descendants
Vav1-Cre Rosa26-mT/mG	*Vav1-mTmG*	No	mem-GFP after Cre recombination	Labeling of hematopoietic cells for analysis or transplantation (donor)
Vav1-Cre Rosa26-DTR	*DTR$^{i\Delta HC}$*	No	-	Genetic ablation of hematopoietic cells by diphtheria toxin injection
Vav1-Cre Rosa26-DTR Cdh5-mTnG	-	No	H2B-GFP (nuclear) and mem-Tdtomato	Genetic ablation of hematopoietic cells by diphtheria toxin injection and labeling of ECs for imaging and FACS
Vav1-Cre VEGFa^{tm2Gne}	*Vegfa$^{\Delta HC}$*	No	-	Knockout of *Vegfa* in hematopoietic cells
Vav1-Cre Kdr^{tm1Wag}	*Vegfr2$^{\Delta HC}$*	No	-	Knockout of *Vegfr2* in hematopoietic cells
Apln-CreERT2 Rosa26-DTA	*DTA$^{i\Delta apln}$*	Yes		Inducible ablation of Apln+ ECs, triggered by tamoxifen

Cdh5(PAC)-CreERT2 Kdr^{tm1Wag}	*Vegfr2$^{i\Delta EC}$*	Yes		Knockout of *Vegfr2* in ECs and their descendants
Apln-CreERT2 Rosa26 Kdr^{tm1Wag}	*Vegfr2$^{i\Delta apln}$*	Yes		Knockout of *Vegfr2* in Apln+ ECs and their descendants
Esm1-CreERT2	-	Yes	-	Labeling of Esm1+ ECs and their descendants
Esm1-CreER Rosa26-mT/mG	-	Yes	mem-GFP after Cre recombination	Labeling of Esm1+ ECs and their descendants for lineage tracing
Esm1-CreERT2 Rosa26-DTA	*DTA$^{i\triangle Esm1}$*	Yes		Genetic ablation of Esm1+ ECs, triggered by tamoxifen
Kitl$^{tm2.1Sjm/J}$				Conditional knockout of stem cell factor (*Kitl*)
Apln-CreERT2 Kitl$^{tm2.1Sjm/J}$	*Kitl$^{i\Delta apln}$*	Yes		Knockout of stem cell factor (*Kitl*) in Apln+ ECs